UNIVERSITÀ DEGLI STUDI DI PADOVA

DEPARTMENT OF CIVIL AND ENVIRONMENTAL ENGINEERING

MASTER THESIS IN WATER AND GEOLOGICAL RISK ENGINEERING

D-CASCADE MODEL APPLICATION IN PREDICTING BED MATERIAL TRANSPORT: ASSESSING THE IMPACT OF SLOPE UNCERTAINTY ON SEDIMENT FLUXES ESTIMATION IN THE PO RIVER

SUPERVISOR
Simone Bizzi

MASTER CANDIDATE
Rafaella Gouveia Loureiro Oliveira

STUDENT ID
2046908

ACADEMIC YEAR 2023/2024

DEDICATION

To my beloved mother, Danielly Gouveia Guedes Loureiro, whose unwavering support and boundless love have shaped the person I am today. Her memory remains eternally cherished in my heart, serving as an everlasting source of guidance and affection.

ABSTRACT

Characterizing sediment fluxes and their evolutionary trends is vital for effective sediment management and river basin planning. The slope is a critical parameter for estimating sediment fluxes. This study investigates how different slope scenarios impact bed material flux modeling in the Po River basin, utilizing the D-CASCADE model, and validates simulated sediment fluxes with two reference datasets—one site-specific and one at the network scale. Four slope scenarios were delineated using diverse DEMs and computation methods, followed by simulations to analyze bed material transport. Discrepancies in model outcomes highlight the sensitivity of sediment flux modeling to slope variations and DEM resolution. Three scenarios exhibit similar bed material flux trends, albeit with varying magnitudes. Simplistic slope computation methods, prone to user subjectivity, led to unrealistic mobilization spikes, which were mitigated by smoothing operations. Finer resolution DEMs increased sediment disconnectivity around the Isola Serafini dam, while coarser resolutions yielded higher mobilized sediment fluxes. The model shows heightened sensitivity to slope variations in lowland areas with higher discharge values. Validation results, falling within the same order of magnitude and variability range as observations, are deemed satisfactory despite uncertainties. The study underscores the D-CASCADE model's utility in simulating sediment fluxes and stresses the necessity for spatially distributed evidence to enhance model calibration and validation. Further sensitivity analyses are deemed crucial for refining model accuracy and reliability.

TABLE OF CONTENTS

LIST OF FIGURES

LIST OF TABLES

CHAPTER 1

1. INTRODUCTION

Bed material transport is a primary driver of channel morphology in alluvial river channels and, thus, influences the formation of various features like bars, pools, riffles, and meanders (Church, 2006). These features, formed through the movement and deposition of bed material, serve as habitats for different aquatic species, influencing biodiversity and ecosystem health. Therefore, characterizing sediment fluxes and their evolutionary trends is critical for effective sediment management and river basin planning.

By analyzing sediment fluxes, policymakers and resource managers can identify sediment sources, sinks, and transport pathways, enabling targeted interventions to mitigate erosion, sedimentation, and associated environmental impacts (Khan et al., 2021). Moreover, understanding these fluxes facilitates the assessment of river system resilience to natural disturbances and anthropogenic pressures, aiding in developing adaptive management strategies to address changing sediment dynamics (Brenna et al., 2024).

Modeling network-scale sediment connectivity requires a delicate balance between simplifying local-scale processes and capturing the primary driving forces and connectivity patterns (Bizzi et al., 2021). Challenges in geomorphic modeling at larger scales include effectively capturing landscape heterogeneity and connectivity patterns, selecting appropriate metrics, and determining the fundamental temporal and spatial scales for the phenomenon of interest to ensure a representative sample of transport events (Wohl et al., 2019).

The slope is a critical parameter in sediment flux estimation because it influences the gravitational force acting on sediment particles. This, in turn, affects the transport capacity of the flow and the likelihood of sediment movement (Pelletier, 2013). Steeper slopes, particularly during high-flow events, can lead to greater erosion and sediment transport by increasing flow velocities and shear stresses, thereby mobilizing and transporting larger sediment particles (Church, 2006). Consequently, characterization of slope is crucial for a realistic estimation of sediment flux and understanding of river

channel morphology over time.

Traditional methods of slope estimation, such as using digital elevation models (DEMs), are susceptible to errors due to uncertainties in data acquisition, interpolation techniques, and spatial resolution (Fisher & Tate, 2006). Infrastructure features such as bridges, culverts, and reservoirs can distort longitudinal river profiles derived from DEMs, potentially masking genuine features or introducing misleading patterns (Schwanghart et al., 2013). One approach to address these challenges is to smooth irregular river profiles, aiming to better reflect elevations and gradients along the river that closely resemble those observed in reality (Schwanghart & Scherler, 2017).

As highlighted by Schoorl et al. (2000), the spatial resolution of the DEM used in modeling significantly influences erosion predictions, emphasizing the importance of accurately representing the landscape extent and relief characteristics. Despite that, there have been numerous studies on the impact of DEM resolution on hydrology, but only a handful have investigated its effects on landscape evolution models (Temme et al., 2013). A finer spatial resolution of the DEM enables a more nuanced representation of the terrain, capturing smaller-scale features and altering the significance of various factors such as slope gradients. Depending on the objectives, methods, and scale of the investigation, this may or may not be the most suitable choice (Lisenby & Fryirs, 2017).

The Dynamic-CAtchment Sediment Connectivity And DElivery (D-CASCADE) model, introduced by Tangi et al. (2022), is an innovative tool for quantifying spatiotemporal sediment connectivity within river networks. This model combines empirical sediment transport formulas with network modeling concepts to simulate sediment transport processes over time. Its potential applications range from reconstructing historical sediment storage and dynamics to forecasting future trends in channel evolution. Moreover, its versatility and scalability make it an interesting tool for exploring intricate sediment connectivity mechanisms.

The Po River is the longest river in Italy and holds significant importance for supporting diverse ecosystems, agricultural activities, and human settlements (Frascaroli et al., 2021). However, human activities such as dam construction and mining have extensively impacted this river over the last century, disrupting sediment distribution and impacting ecological quality (Brenna et al., 2024; Parrinello et al., 2021; Surian & Rinaldi, 2003). To ensure the resilience of the river ecosystem amidst anthropogenic

influences, it is important to understand sediment transport patterns to implement sustainable river management practices.

This study utilizes the D-CASCADE model in the Po River basin to simulate bed material fluxes at a network scale. It employs various methods of slope extraction from the river network, utilizing both a widely available national DEM of intermediate resolution (10 m) and a high-resolution (1 m) LiDAR-derived DEM. This research aims to validate simulated sediment fluxes using available data and field evidence in the Po River; and examine the impact of different slope scenarios on sediment flux estimation using the D-CASCADE model.

CHAPTER 2

2. DATA AND METHODS

2.1. Study area

The study area is the Po River basin (Figure 1), which stands as Italy's largest river basin, covering a drainage area of 70,091 km² and extending across seven Italian regions along with approximately 3,200 municipalities (Bozzola & Swanson, 2014). The Po River flows over 650 kilometers, from the Monviso mountain in the Piedmont region to the Adriatic Sea in the Emilia Romagna region, and presents a mean annual discharge of approximately 1,500 m³/s (Parrinello et al., 2021).

The basin is dominated by the Po River, the longest river in Italy, and its network of tributaries, including the Ticino, Adda, Oglio and Mincio rivers. This region is one of the most densely populated, cultivated, and developed regions in Italy (Bozzola & Swanson, 2014). The catchment comprises a diverse range of terrains, featuring mountainous areas in the northern region and fertile plains in the southern part. This varied landscape contributes significantly to the basin's abundant biodiversity (Bozzola & Swanson, 2014). Its pluviometric regime is characterized by distinct patterns of rainfall distribution throughout the year, with an average of 1,200 mm (Montanari, 2012).

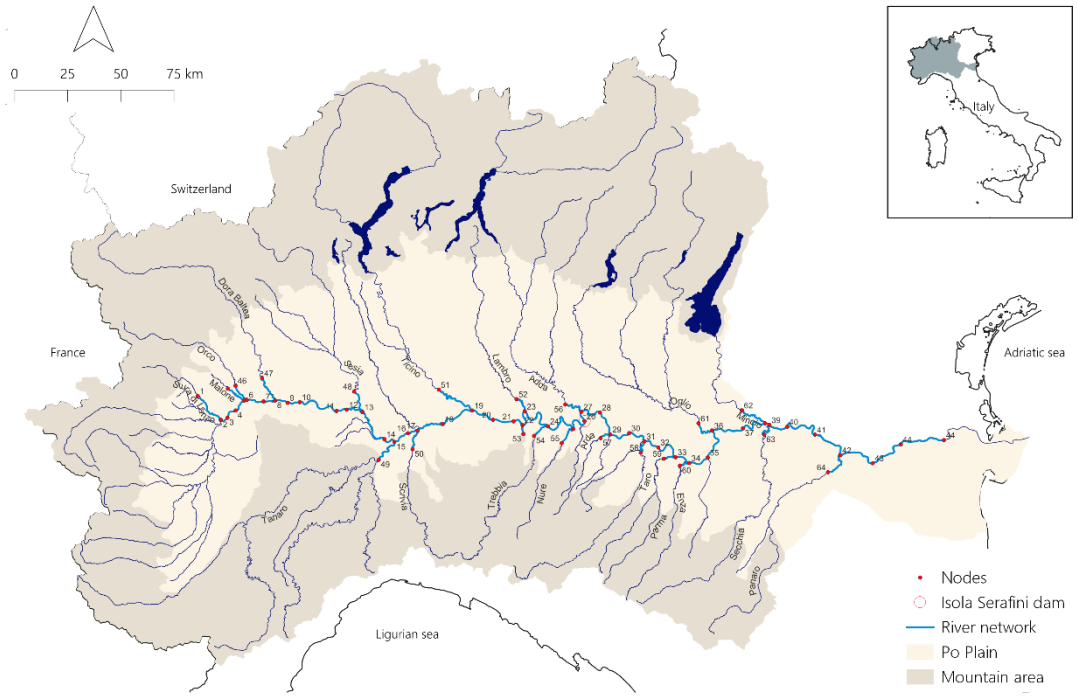

Figure 1. The Po River catchment, featuring the river network (and its nodes) considered in this study.

From the 1960s to the 1970s, human interventions aimed at exploiting sediment and water resources led to a reduction in sediment availability along the river, which combined with the implementation of river training works to ensure navigability, caused significant changes in the channel morphology (Brenna et al., 2024; Surian & Rinaldi, 2003). These activities have led to consequences such as changes in natural flow patterns, sediment transport disruptions, channel incision, bank erosion, and habitat degradation (Surian & Rinaldi, 2003).

One of the most relevant examples of these interventions is the Isola Serafini dam, which is a run-of-river hydropower plant, operational since 1962, that diverts part of the river flow to four vertical Kaplan turbines with a total capacity of 80 MW (Bizzi et al., 2015). This modification, coupled with human activities like instream sand mining, has accelerated riverbed degradation in the middle-lower course of the Po River (Bizzi et al., 2015).

In this context, the renaturation project of the Po River was introduced in 2021 by the *Autorità di bacino distrettuale del fiume Po,* which is the the Po River basin authority. This initiative stands as one of Italy's most important river restoration initiatives,

supported by funding from the National Recovery and Resilience Plan (PNRR). The main goal of this project is to restore the ecological balance and biodiversity of the Po River catchment. This involves implementing measures to improve the natural habitats, ecosystems, and overall environmental quality of the region, through habitat restoration, reforestation programs, and initiatives to enhance the natural landscape (AdbPo, 2022). These restoration efforts have the potential to enhance sediment retention, reduce erosion, and improve sediment balance, contributing to a more sustainable and resilient sediment transport regime in the Po River basin (AdbPo, 2008).

2.2. D-CASCADE model

2.2.1. Model description

The Dynamic-CAtchment Sediment Connectivity And DElivery (D-CASCADE) model introduced by Tangi et al. (2022) operates on a network scale, aiming to replicate the temporal and spatial progression of sediment supply and distribution within river basins. This model extends the CASCADE framework (Schmitt et al., 2016), which delineates the movement of sediment from distinct sources through individual transport processes referred to as "cascades", by adding dynamic components. Each cascade is distinguished by its point of origin and transports a defined sediment volume that may undergo partial or complete deposition as it progresses downstream and interacts with other cascades.

As described by Tangi et al. (2022), the D-CASCADE model comprises two primary phases: initialization and the primary D-CASCADE loop, each characterized as follows. In the initialization phase, the model establishes the necessary input data and outlines the structure of the simulation. This involves representing the river network as a graph with nodes and reaches, where each reach signifies a segment of the river network with distinct geomorphic and hydraulic attributes.

Throughout the main D-CASCADE loop, the model's dynamic framework operates, tracking the movement of sediment cascades across time and space. This phase encompasses a series of operations repeated for each reach and at each timestep. These operations include defining mobilized sediment, assessing changes in geomorphic

features, and determining sediment delivery (Tangi et al., 2022).

In defining mobilized sediment, the total volume of sediment mobilized and transported downstream during each timestep comprises cascades received from upstream in the previous timestep, those held in the deposited layer, or a combination of both (Tangi et al., 2022). The deposited layer is conceptualized as a stack of distinct tiers, with each tier representing a single cascade. The approach of D-CASCADE ensures that newly deposited cascades form a tier above previously deposited material, while entrained sediment is removed from the upper tiers of the deposit.

Figure 2 illustrates the steps in determining the mobilized sediment volume for a specific reach. The colors of the tiers in (a) represent the reach of origin within the network. As defined by Tangi et al. (2022), in (b), the model identifies incoming cascades and the deposit layer during the timestep. In (c), the deposit is divided into active and substrate layers. Subsequently, in (d), the model computes the transport capacity for sediment in the active layer based on the layer's Grain Size Distribution (GSD). Finally, in (e), the mobilized volume and new deposit layer are established.

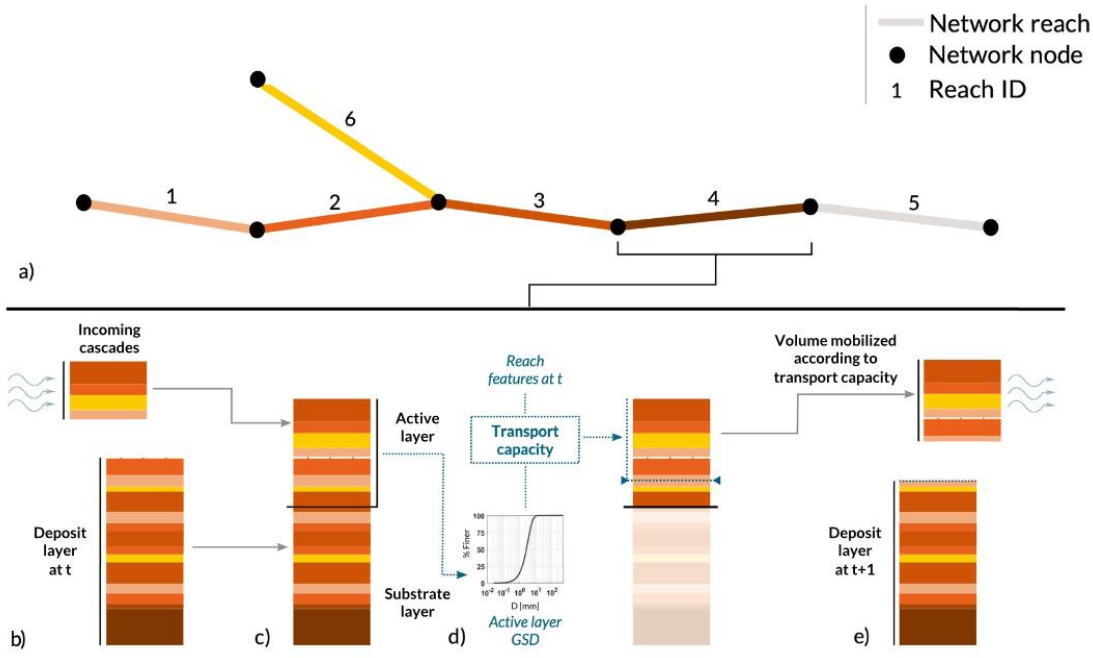

Figure 2. Definition of mobilized sediment volume within a reach during a single timestep in the D-CASCADE model. Source: Tangi et al., 2022.

2.2.2. Applications

Recent studies have showcased the D-CASCADE potential applications in modeling sediment connectivity (Bizzi et al., 2021; Schmitt et al., 2016, 2018, 2021; Tangi et al., 2022). This model has been used to quantify bed material sediment fluxes, track sediment deposition and delivery, assess scenarios of hydropower production with respect to sediment connectivity, and reconstruct historical geomorphological changes in river networks. Moreover, the model is adaptable for forecasting future trajectories of sediment transport patterns and evaluating the efficacy of various management strategies in mitigating sediment-related challenges (Schmitt et al., 2016).

2.2.3. Required inputs and parameters

The D-CASCADE model requires some key inputs, listed in Table 1. Reach characteristics encompass slope, length, width, and roughness coefficient. Hydrological aspects are integrated into the model through the inclusion of discharge input, while sediment characterization is performed by analyzing the distribution of grain sizes.

Table 1. Key inputs required for the D-CASCADE model organized by relevant categories.

Reach characterization	***Hydrology***	***Sediment characterization***
Slope (m/m)	Discharge (m^3/s)	Grain size distribution (i.e., D16, D50, D84) (mm)
Width (m)		
Length (m)		
Manning's coefficient (n)		

Table 2 presents the user-defined parameters required by the model along with their values adopted in this study. The maximum active layer is defined as the maximum height of mobilized sediment volume within a reach during a single timestep. This parameter is

crucial for determining the depth of the sediment layer that is actively transported and redistributed within the river network. The maximum active layer volume serves as a limit on the amount of sediment that can be mobilized and transported downstream in each timeframe. By setting a maximum active layer volume, the model can simulate realistic sediment transport processes and ensure that the amount of sediment mobilized aligns with the hydraulic and geomorphic conditions of the river reaches, contributing to the accurate representation of sediment connectivity and dynamics in the D-CASCADE simulations (Tangi et al., 2022).

Table 2. Key user-defined parameters required for the D-CASCADE model.

Parameter	***Value***
Maximum active layer (m)	0.3
Sediment classes (ϕ scale)	(-8, 5)
Initial deposit (m^3/m)	100,000

The sediment classes are defined as the range of sediment sizes considered in the model. The initial deposit represents the total amount of sediment stored within each reach at the beginning of the computation. The determination of the initial deposit and maximum active layer should rely on field surveys and expert assessments (Tangi et al., 2022). Nevertheless, acquiring such data is frequently challenging, as observed in this study, resulting in uncertainty in the estimation of these parameters.

An effective description of these parameters within the D-CASCADE model significantly influences the accuracy and reliability of its outputs. Proper parametrization ensures a reliable representation of physical processes and interactions within the river network, thereby yielding more realistic simulations of sediment transport and connectivity dynamics (Schmitt et al., 2016).

2.2.4. Transport capacity computation

The selection of a sediment transport formula significantly influences the results of the

model. Choosing an appropriate formula that corresponds to observed sediment transport phenomena enables better calibration of the model to align with real-world data (Church, 2006), thus enhancing its reliability and accuracy. That said, the Engelund and Hansen sediment transport formula was used in the D-CASCADE simulations as it is suitable for the Po River, which is sand-bedded throughout most of its length (Brenna et al., 2022).

The sediment transport empirical formula developed by Engelund and Hansen (1967) stands as a widely embraced relationship used for computing sediment transport within alluvial streams. This equation furnishes an approximation of the sediment transport rate grounded on flow conditions and sediment attributes. Their data collection efforts encompassed sediment transport rates across diverse flow conditions, channel slopes, and sediment characteristics, aiming to grasp the factors influencing sediment movement. These empirical findings, coupled with theoretical insights from fluid mechanics and sediment transport, culminated in the development of a mathematical relationship capable of elucidating the sediment transport process in rivers.

The equation's development relies in thorough flume observations, primarily centered on sediment sizes ranging from 0.19 mm to 0.93 mm, which encompasses fine to coarse sand. Through a blend of empirical observations and theoretical considerations pertaining to sediment dynamics in rivers, Engelund and Hansen (1967) developed the following formula:

$$gs = V^2 \left(\frac{\tau b}{(\gamma s - \gamma)\, d50}\right)^{\frac{3}{2}} \sqrt{\frac{d50}{g\left(\frac{\gamma s}{\gamma} - 1\right)}} = V^2 (\tau^*)^{\frac{3}{2}} \sqrt{\frac{d50}{g\left(\frac{\gamma s}{\gamma} - 1\right)}}$$

Where:

gs = Sediment transport;
γ = Unit weight of water;
γs = Unit weight of sediment;
V = Average channel velocity;
τb = Bed shear stress;
τ^* = Dimensionless Shields Number;
$d50$ = Median particle size.

In addition, the bed material fraction method was used as a technique, in conjunction with the Engelund and Hansen formula, to partition the total sediment transport into

different size fractions based on the sediment characteristics (Molinas & Wu, 2000), in order to better represent how different fractions contribute to channel erosion, and deposition processes, thereby improving predictions of morphological changes over time and enhancing the understanding of sediment connectivity within the river network (Tangi et al., 2022).

Nonetheless, it is important to acknowledge that this equation might not address the spatial heterogeneity inherent in sediment transport processes within a river network, due to the variations of grain size. Consequently, employing this equation on a network scale could oversimplify the intricate sediment transport dynamics, introducing uncertainties when estimating sediment transport rates.

2.3. Data

2.3.1. Digital elevation models (DEM)

For this study, two different DEMs were used to obtain the slope scenarios. The first one is a nationally available DEM of 10 meters spatial resolution, generated in 2005, consisting of bare ground elevation. The elevation data used as input to generate this DEM comes from several sources, including contour lines and spot heights derived from regional topographic maps, satellite-based global positioning system points, and ground-based and radar altimetry (Tarquini et al., 2007). Additionally, the Po River Basin Authority (AdbPo) provided a LiDAR-derived DEM with a 1-meter spatial resolution, collected in 2021 from an airplane acquisition.

2.3.2. River reaches

To conduct the D-CASCADE simulation, the river network underwent partitioning into distinct reaches, guided by specific criteria to ensure geomorphological homogeneity within each segment. Figure 3 illustrates the Po River network, delineating the location of each reach, with numerical markers denoting the reach nodes. Table 1 provides detailed characteristics of each reach, such as upstream and downstream nodes, length, width, and grain size distribution. For clarity and reference, in the following sections, each reach was

associated with its respective upstream node.

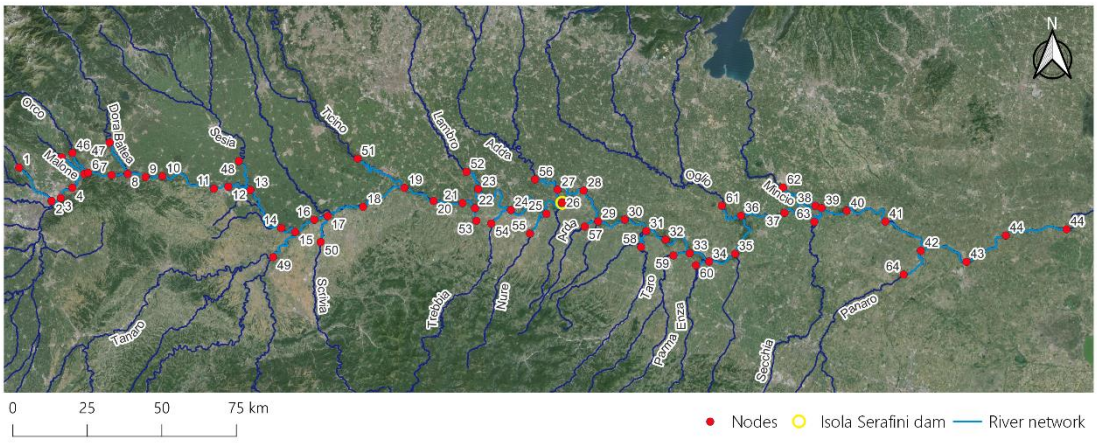

Figure 3. Simulated Po River network with the main tributaries included. Numerical markers denote the reach nodes.

Table 3. River reach characteristics including upstream and downstream nodes, length, width, and grain size distribution.

River	Upstream Node	Downstream Node	Reach	Length (m)	Width (m)	Grain size (mm)		
						D16	D50	D84
Po	2	3	PO_2	3965	170	1.602	19.094	40.440
Po	3	4	PO_3	6015	101	1.602	19.094	40.440
Po	4	5	PO_4a	6904	169	7.454	23.337	40.791
Po	5	6	PO_4b	1388	209	7.454	23.337	40.791
Po	6	7	PO_5	8630	169	3.367	20.910	39.918
Po	7	8	PO_6	6099	196	1.200	21.741	54.550
Po	8	9	PO_7	6681	163	1.180	10.417	27.516
Po	9	10	PO_8	6116	178	12.090	33.890	45.850
Po	10	11	PO_9	22342	177	1.079	11.645	40.560
Po	11	12	PO_10	5443	170	2.105	54.981	78.980
Po	12	13	PO_11	9738	183	0.643	30.133	67.644
Po	13	14	PO_12	21608	331	2.303	17.605	54.054
Po	14	15	PO_13	7165	235	2.848	20.690	58.357
Po	15	16	PO_14	8625	359	0.785	4.784	16.950
Po	16	17	PO_15a	5299	460	5.393	19.320	41.841

Po	17	18	PO_15b	14515	427	2.483	11.067	29.000
Po	18	19	PO_16	18391	313	1.227	2.392	20.110
Po	19	20	PO_17	11833	440	0.500	2.392	17.718
Po	20	21	PO_18	10127	383	0.495	0.693	21.891
Po	21	22	PO_19a	5678	342	0.621	1.060	20.819
Po	22	23	PO_19b	8761	309	0.757	2.379	22.461
Po	23	24	PO_19c	21620	331	0.757	2.379	22.461
Po	24	25	PO_20a	20158	291	0.507	0.798	1.126
Po	25	26	PO_20b	11852	361	0.507	0.798	1.126
Po	26	27	PO_21a	5191	340	0.548	2.370	5.865
Po	27	28	PO_21b	12388	321	0.288	1.756	4.216
Po	28	29	PO_22	12427	303	0.249	2.519	24.840
Po	29	30	PO_23	10644	301	0.302	0.599	9.552
Po	30	31	PO_24	10560	272	0.273	0.611	5.050
Po	31	32	PO_25	8167	309	0.344	0.669	7.215
Po	32	33	PO_26	14531	276	0.248	0.347	0.465
Po	33	34	PO_27a	7697	270	0.318	0.490	9.422
Po	34	35	PO_27b	10379	259	0.293	0.390	0.667
Po	35	36	PO_28	16559	333	0.297	0.397	0.599
Po	36	37	PO_29	16514	382	0.241	0.347	0.552
Po	37	38	PO_30	14987	362	0.272	0.412	0.627
Po	38	39	PO_31a	2250	340	0.295	0.395	0.603
Po	39	40	PO_31b	9562	416	0.290	0.388	0.594
Po	40	41	PO_32	21677	361	0.270	0.372	0.573
Po	41	42	PO_33	17964	454	0.272	0.345	0.562
Po	42	43	PO_34	19235	383	0.238	0.334	0.466
Po	43	44	PO_35	18390	377	0.289	0.349	0.483
Po	44	44	PO_36	22149	358	0.203	0.283	0.397
Stura di Lanzo	1	2	STURA DI LANZO_1	18290	147	1.602	19.094	40.440
Malone	45	5	MALONE_1	11669	47	7.454	23.227	40.791
Orco	46	6	ORCO_1	9383	124	3.367	20.910	39.918
Dora Baltea	47	8	DORA BALTEA_1	14790	103	1.188	10.417	27.516
Sesia	48	13	SESIA_1	12767	118	2.303	17.605	54.053
Tanaro	49	15	TANARO_1	15554	107	0.786	4.786	16.950

Scrivia	50	17	SCRIVIA_1	11000	29	2.483	11.067	29.000
Ticino	51	19	TICINO_1	25021	144	0.500	2.392	17.718
Lambro	52	23	LAMBRO_1	8758	53	0.757	2.379	22.461
Tidone	53	22	TIDONE_1	4799	20	0.755	2.379	22.461
Trebbia	54	24	TREBBIA_1	9469	196	0.507	0.798	1.126
Nure	55	25	NURE_1	11037	19	0.507	0.798	1.126
Adda	56	27	ADDA_1	12457	113	0.288	1.756	4.216
Arda	57	29	ARDA_1	5483	10	0.302	0.599	9.552
Taro	58	31	TARO_1	9867	56	0.344	0.669	7.214
Parma	59	33	PARMA_1	8156	14	0.318	0.481	9.422
Enza	60	34	ENZA_1	5967	12	0.293	0.390	0.667
Oglio	61	36	OGLIO_1	12510	97	0.241	0.347	0.552
Mincio	62	38	MINICIO_1	15324	42	0.291	0.391	0.603
Secchia	63	39	SECCHIA_1	12881	18	0.290	0.388	0.594
Panaro	64	42	PANARO_1	14296	18	0.238	0.334	0.466

It is worth mentioning that the width was assumed to be constant and equivalent to the active channel width, derived from satellite images from 2022, which accounts for the area occupied by low flow channels and unvegetated bars. However, this representation may underestimate sediment transport processes, as the actual channel width conducive to sediment transport may be narrower than the maximum width considered in the model, particularly during low flow rate timesteps.

2.3.3. Grain size

The grain size distribution along the river reaches was derived from field measurements conducted by the Po River Basin Authority (AdbPo) during the development of the sediment management plan between 2005 and 2008. Due to the absence of grain size field measurements for the tributaries, a simplification was implemented whereby their characteristics were assumed to match those of the downstream reach of the Po River. Figures 4 and 5 illustrate the box plots representing the D50 and D84 values obtained from these measurements for each reach.

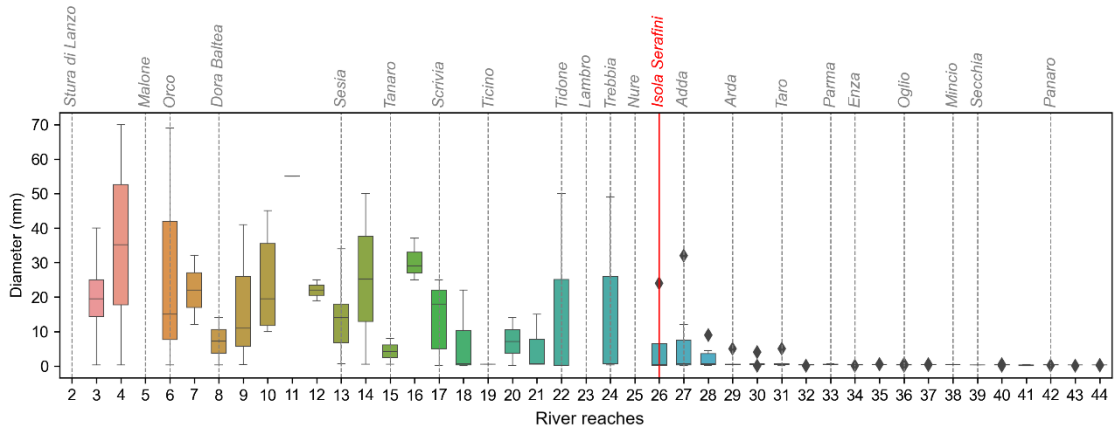

Figure 4. Box plot illustrating the distribution of D50 field measurements across all river reaches.

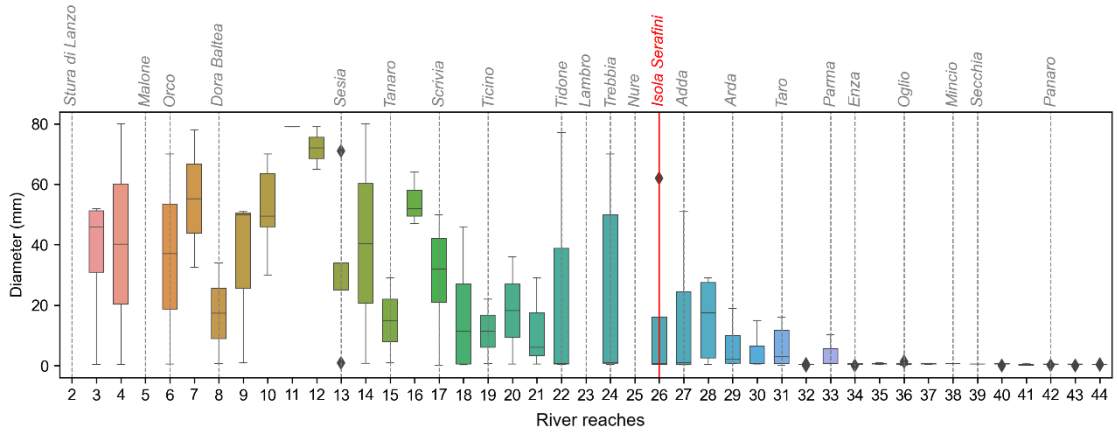

Figure 5. Box plot illustrating the distribution of D84 field measurements across all river reaches.

Especially the D50 parameter holds significant importance as it offers a measure of the central tendency of the grain size distribution (Schmitt et al., 2018). This parameter is commonly utilized to characterize the average size of sediment particles in a sample and is crucial for comprehending sediment transport processes, erosion rates, deposition patterns, and overall sediment dynamics in river systems (Schmitt et al., 2018). In the context of the D-CASCADE model, D50 plays a key role in determining sediment transport capacity, channel morphology changes, and the spatiotemporal evolution of sediment connectivity within river networks (Tangi et al., 2022).

To determine a more suitable grain size distribution input for the model, a weighted average was computed based on the initial D16, D50, and D84 data. Samples collected

from the wetted areas of the reach were accorded greater significance relative to those obtained from the bars. The outcomes of this procedure for each reach are delineated in Table 3.

2.3.4. Discharge

Discharge data plays a fundamental role in the D-CASCADE model, providing the hydrological information required for accurately computing transport capacity within river networks (Schmitt et al., 2016). Integrating discharge data time series enhances the ability of the model to simulate the impact of flow rates on sediment transport pathways, erosion, and deposition, thereby enriching the representation of sediment connectivity (Tangi et al., 2022).

The discharge data was derived from the Flood-PROOFS probabilistic forecasting system (Laiolo et al., 2014), which employs a rainfall-runoff model known as DRiFt. This model incorporates real-time MODIS sensor data and snow depth measurements to ensure accurate forecasting. It initializes soil moisture conditions based on an Antecedent Precipitation Index (API) and satellite-based estimates of soil moisture, thereby enhancing its predictive capabilities. It is worth mentioning that this system has been adapted to account for the presence of dams and other hydraulic structures.

The values of discharge associated with each reach, for a period spanning from 2019 to 2021, were given by the International Center for Environmental Monitoring (CIMA) foundation, which is working in collaboration with UNIPD on several ongoing research projects involving the mentioned system.

2.3.5. Slope scenarios

Several slope scenarios were evaluated, but the following four were deemed particularly significant for discussion. Simulation results for the remaining scenarios are in the appendix of this work.

Scenario I: Slope derived from a first approach using the 10-meter resolution DEM

The first method of slope computation entailed sampling the nodes elevation from the 10-meter resolution DEM. Subsequently, the slope was derived by dividing the elevation differences between upstream and downstream nodes by the length of the reaches.

Scenario II: Slope derived from polynomial regressions using the 10-meter resolution DEM

The second approach of slope computation also utilized the 10-meter-resolution DEM. Initially, the data from each pixel of the DEM intersecting the Po River network were extracted to facilitate the creation of a polynomial regression model of degree 3. Given the elevation profile disruption caused by the Isola Serafini Dam along the Po River, it became necessary to partition the river network into two segments, distinguishing between reaches situated before and after the dam.

Utilizing the two polynomial regressions (Figure 6) for these segments, new elevation values were computed for each node. Subsequently, the slope was determined by calculating the difference in elevation between the upstream and downstream nodes within each reach and dividing it by the length of the respective reach.

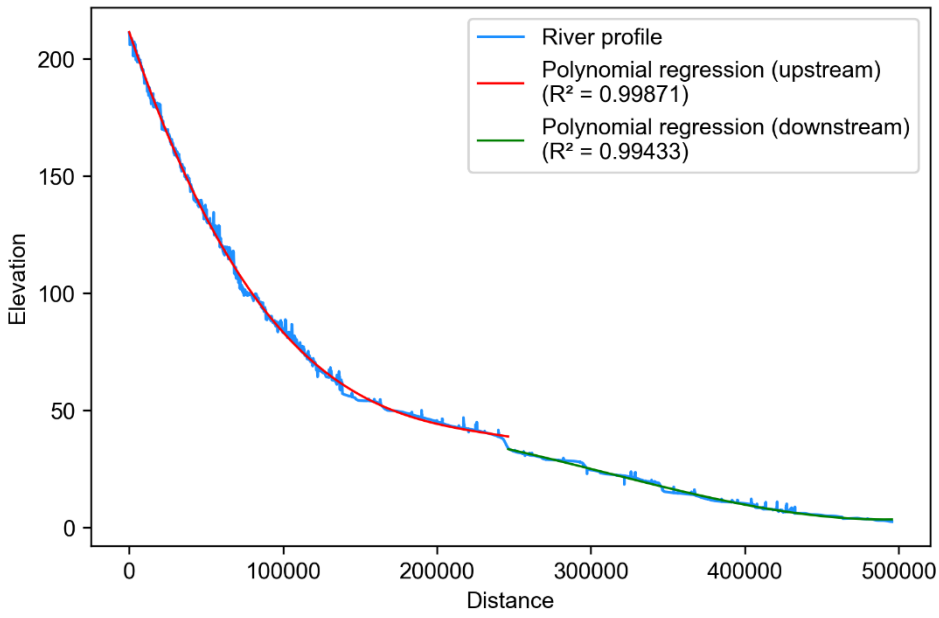

Figure 6. River profile alongside polynomial regressions fitted to the 10-meter resolution Digital Elevation Model (DEM).

Scenario III: Slope derived from polynomial regressions using the 1-meter resolution DEM

The procedure for obtaining the slope for this scenario mirrored that described for Scenario II, utilizing the 1-meter resolution DEM instead. Polynomial regression analysis of degree 3 was again employed by segmenting the network into pre-dam and post-dam sections (Figure 7). Then, refined elevation values were computed for each node along the river network. Subsequently, slope calculations were performed by assessing the difference in elevation between adjacent nodes within each reach and dividing it by the length of the respective reach.

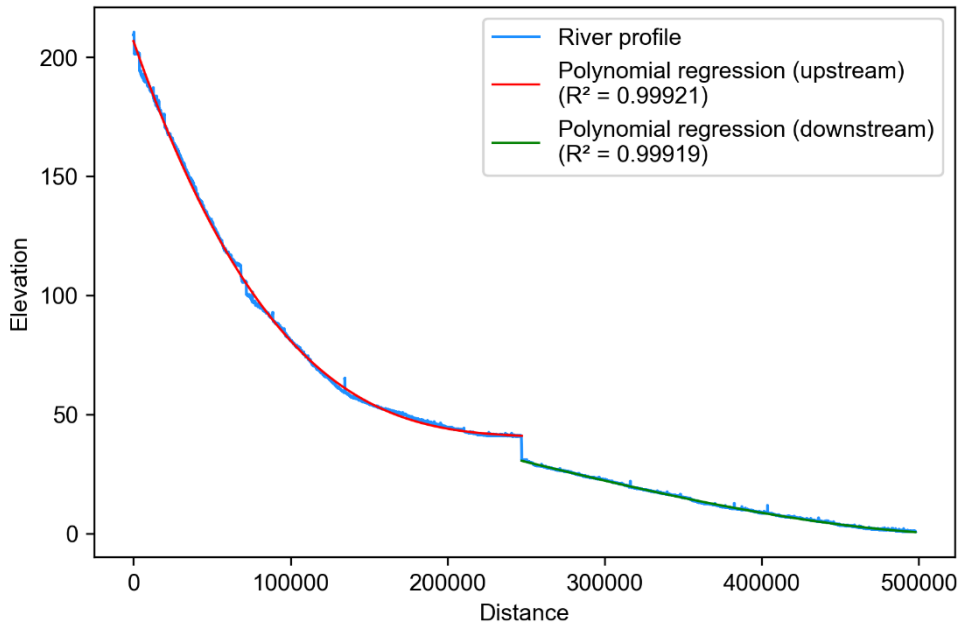

Figure 7. River profile alongside polynomial regressions fitted to the 1-meter resolution Digital Elevation Model (DEM).

Scenario IV: Slope derived from polynomial regressions using the 1-meter resolution DEM (upstream) + Hydraulic slope (downstream)

Furthermore, an additional scenario was formulated using a modeled hydraulic slope provided by the Po River Basin Authority (AdbPo). However, a gap existed in parts of

the dataset due to the absence of slope values for reaches preceding node 13, as well as Reaches 25, 43, and 44. To address this, the missing slope values were filled with slopes obtained for Scenario III. To address this, the missing slope values were filled with slopes obtained from Scenario III. Consequently, the upper part of the Po predominantly comprises slopes from Scenario III, while downstream incorporates the slopes from the hydraulic simulation.

2.3.6. Validation

Given the scarcity of sediment flux field evidence for Italian rivers, particularly at the scale of the Po River network, two primary data sources served as reference points for the validation process.

The first source was a study conducted by Schippa (2021), focusing on bed load and suspended sediment flux measurements at a specific site along the Po River. These measurements were conducted under four different water discharge conditions on four separate dates (13/11/2019, 10/12/2019, 28/1/2021, and 10/2/2021), with discharges ranging between 1300 and 1800 m^3/s. The location of these measurements is depicted in Figure 8. The equivalent of this reach in this simulation is Reach 33 (PO_27a).

Figure 8. Area where the sediment flux measurements were performed. Adapted from UNIFE - Prof. Schippa, 2021, "Studio della morfologia del fondo e degli effetti sul campo di moto e sul trasporto solido nel tratto intermedio del fiume Po".

The second dataset utilized for validation comprised the mean annual sediment budget for the Po River, calculated over a 23-year period (1982-2005), shown in Figure 9. This data was obtained from the sediment management plan (PGS) project conducted between 2005 and 2008. The assessment was formulated using a combination of DEM of Differences (DoD) and transport capacity computations based on a transport-limited hypothesis, with full supply. It is noteworthy that this is the only information available at the entire Po River scale.

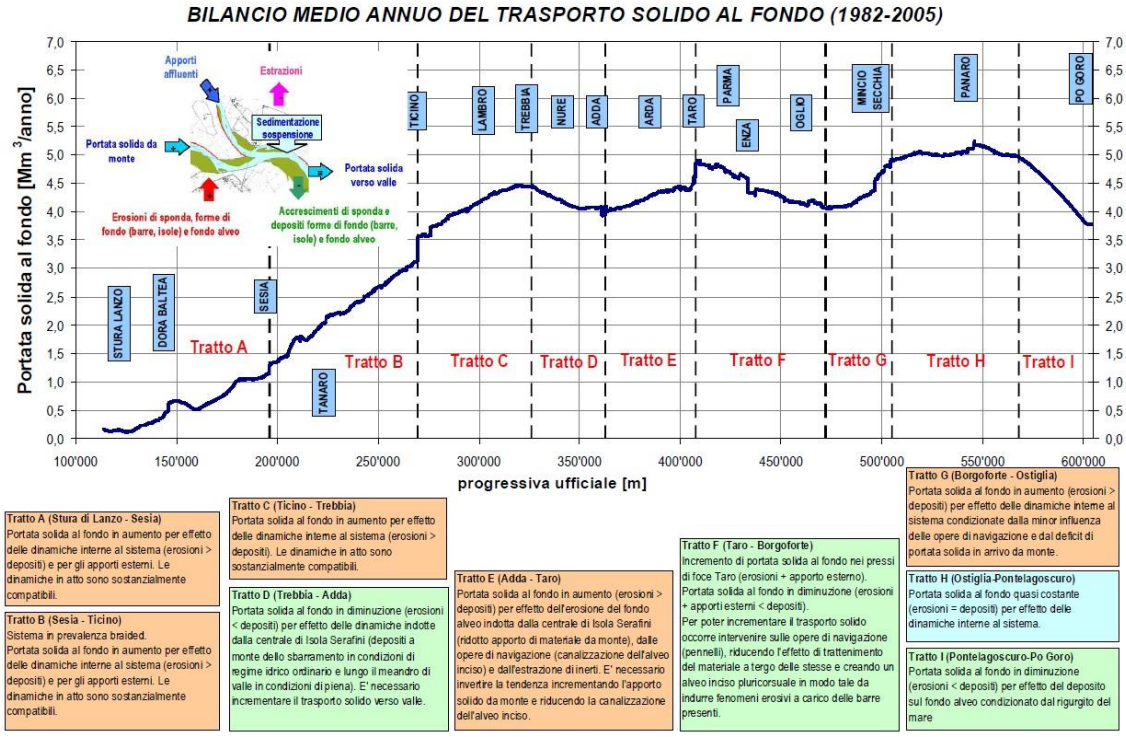

Figure 9. Mean annual budget of bed material flux for the Po River (1982 - 2005) (PGS 2005-2008, AdbPo).

CHAPTER 3

3. RESULTS

In this study, four slope scenarios are assessed for their implications in bed material flux modeling within the Po River basin, employing the D-CASCADE model. The results are validated using two datasets as reference benchmarks. The following sections present the main findings from the conducted simulations and validation.

3.1. Slope Scenario I

Figure 10 displays the mobilized volume found for the first slope scenario, derived from the differences in elevation between the upstream and downstream nodes sampled from the 10-meter resolution DEM.

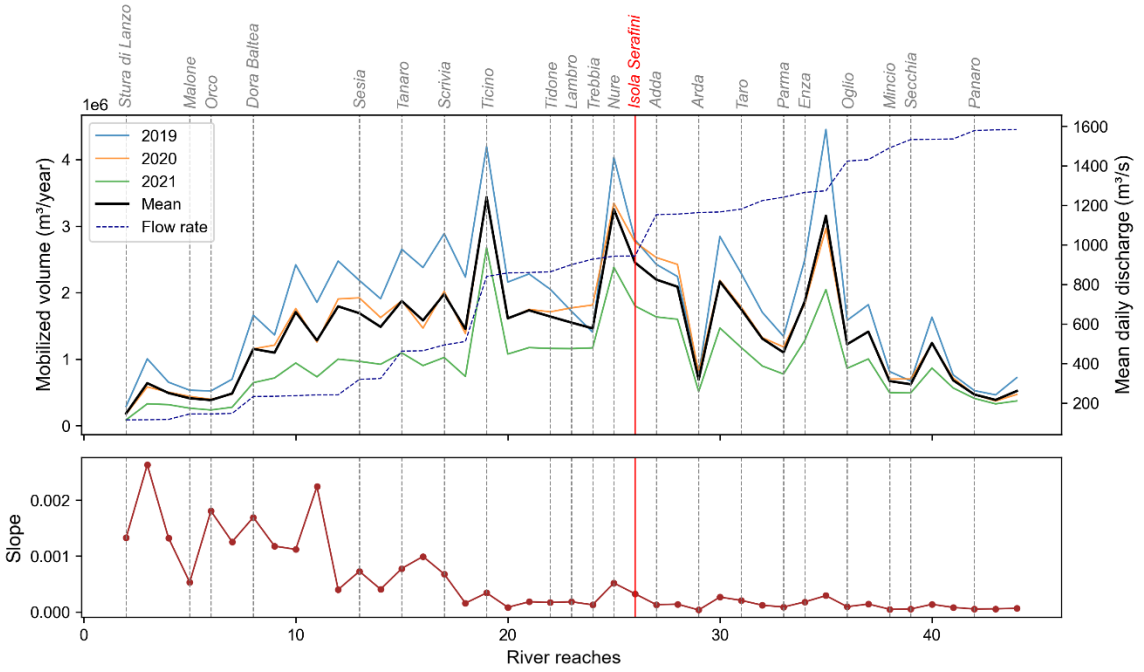

Figure 10. Mean annual mobilized volume, mobilized volume per year, mean daily flow rate, and the corresponding slopes across all reaches, depicted for Scenario I (Initial approach using 10m DEM).

In this scenario, a significant variation in slope is evident, particularly in the upper reaches of the river (prior to Ticino). Although slope values are notably higher and exhibit considerable variability upstream, the most pronounced peaks of mobilization occur only after the midsection of the Po River (between Ticino and Secchia), coinciding with increased discharge. Considering the mean annual value of mobilized volume for the period, the highest peak was of 3,4 M m³/year, in Reach 19. Besides this reach, there are two other prominent spikes of mobilization observed in Reaches 25 and 35, rising up to 4,4 M m³ in 2019.

3.2. Slope Scenario II

Figure 11 displays the mobilized volume found for the second slope scenario, derived using polynomial regression applied to elevation data extracted from the 10-meter resolution DEM across the river network.

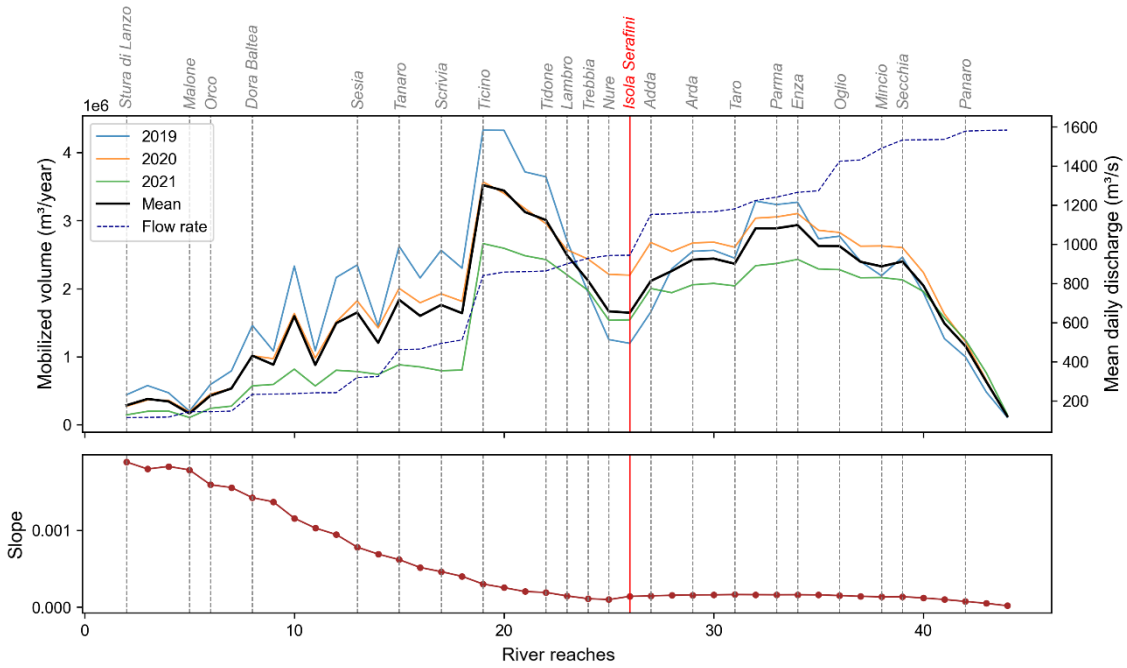

Figure 11. Mean annual mobilized volume, mobilized volume per year, mean daily flow rate, and the corresponding slopes across all reaches, depicted for Scenario II (Polynomial regression using 10m DEM).

In this scenario, a modest fluctuation in slope between consecutive reaches facilitates

a seamless transition from steep gradients upstream to gradually stabilizing slopes downstream. The slope consistently decreases until the Isola Serafini dam, where it experiences a discrete increase before resuming its ascent until Reach 32, where it begins to decline slightly once more.

The highest peak of bed material flux was observed at the river confluence with Ticino, with volumes ranging from 2,6 M to 4,3 M m³/year, averaging at 3,5 M m³/year. This peak coincided with a significant increase in flow rate. Subsequently, sediment mobilization declined to an average rate of 1,6 M m³/year, where the Isola Seranifi dam is situated, after which it began to rise again. An average mobilized volume of around 2,5 M m³/year can be seen in the middle section of the Po after the dam. After the confluence of Secchia, the mobilized volume decreases significantly until it reaches the most downstream reach. Interestingly, between Reaches 24 and 32 and between Reaches 35 and 42 higher sediment transport rates are shown for 2020 than for 2019, even though the discharge presented higher peaks in the first year, as depicted in Figure 12.

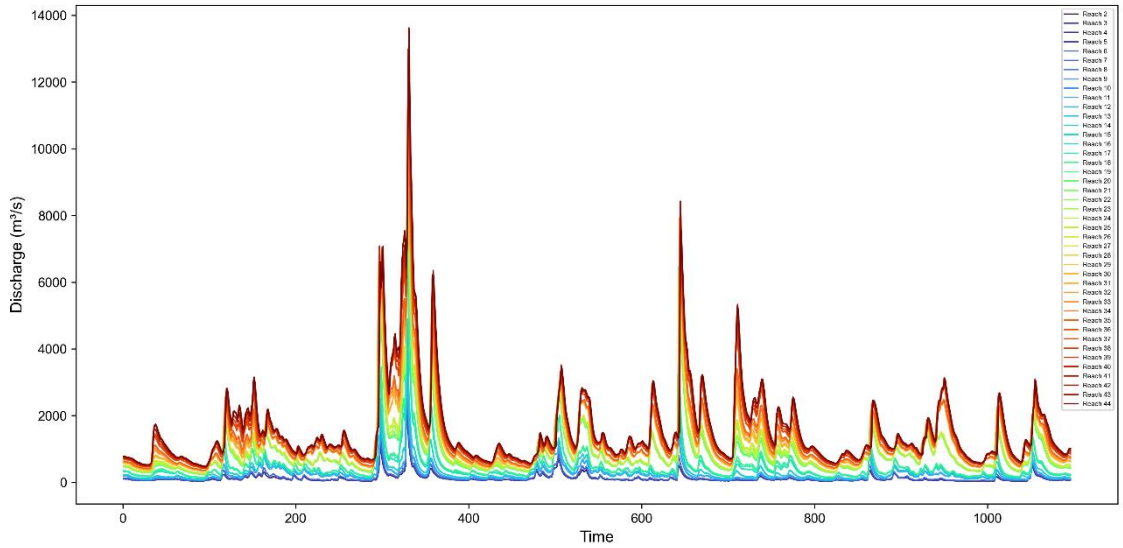

Figure 12. Temporal variation of discharge for each reach.

3.3. Slope Scenario III

Figure 13 displays the mobilized volume found for the third slope scenario, derived using polynomial regression applied to elevation data extracted from the 1-meter

resolution DEM across the river network.

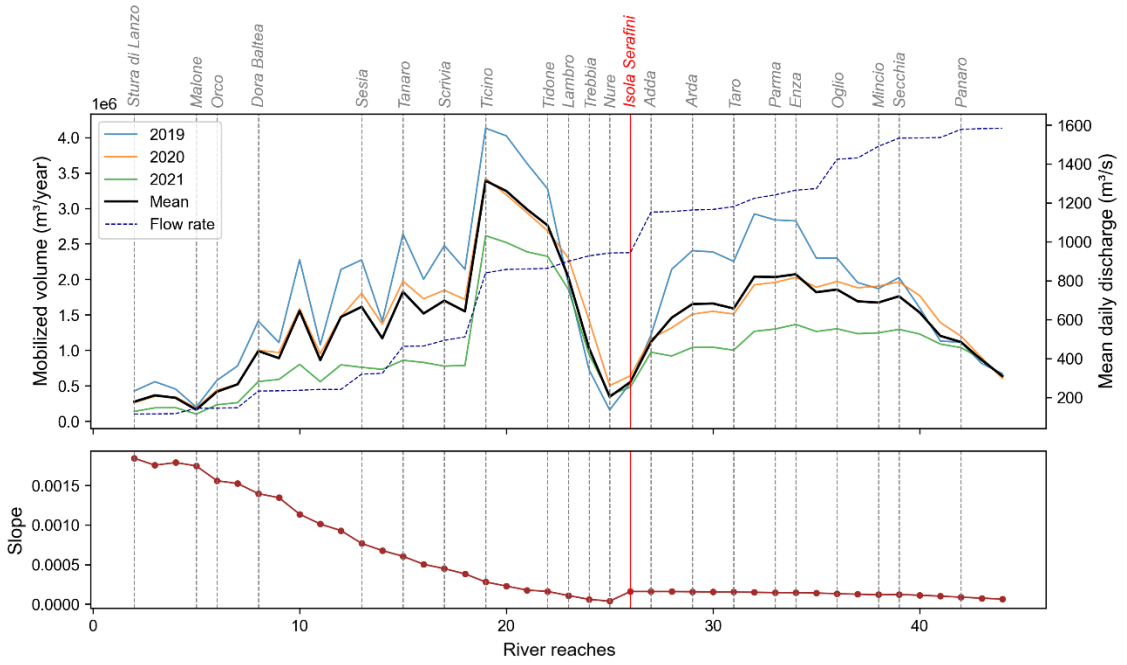

Figure 13. Mean annual mobilized volume, mobilized volume per year, mean daily flow rate, and the corresponding slopes across all reaches, depicted for Scenario III (Polynomial regression using 1m DEM).

Similar to Scenario II, the slope undergoes a gradual transition from steep gradients upstream to gentler slopes downstream, with one notable exception observed at Reach 25. In this specific area, the slope experiences a significant reduction, consistent with the presence of a dam and the associated backwater effects. Coinciding with this diminished slope, the lowest mobilized flux for this slope scenario was observed in Reach 25, totaling 350,000 m³/year. Conversely, the highest peak of mobilization, reaching 3,4 M m³/year, was recorded at Reach 19, situated at the confluence of the Ticino River. Downstream of the dam, in the middle section of the Po River, an average mobilized volume of approximately 1,5 M m³/year is evident.

Additionally, a noteworthy similarity to the previous scenario is the observation that certain reaches (specifically between Reaches 23 and 26) exhibit higher sediment transport rates for 2020 compared to those observed in 2019. Section 3.5.1 will provide further discussion on this phenomenon.

3.4. Slope Scenario IV

Figure 14 exhibits the mobilized volume observed for the fourth slope scenario, which integrates the slope derived from scenario III with the hydraulic slope derived from HEC-RAS simulation. As mentioned in Section 3, the hydraulic slope was applied to all reaches following Reach 13, excluding Reaches 25, 43, and 44.

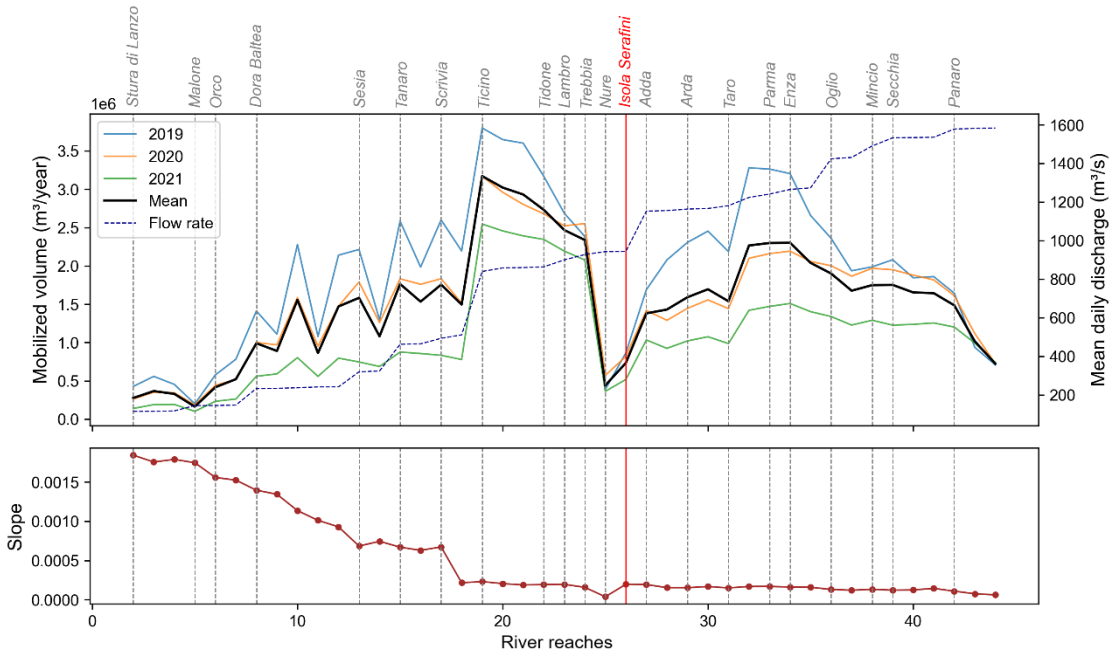

Figure 14. Mean annual mobilized volume, mobilized volume per year, mean daily flow rate, and the corresponding slopes across all reaches, depicted for Scenario IV (Polynomial regression using 1m DEM plus hydraulic slope).

The peak of mobilization was 3,1 M m³/year in the confluence of Ticino. After this peak, mobilization decreases gradually. However, because of the discontinuity of the hydraulic slope data at Reach 25, sediment flux descends steepest in this reach, from a value of 2,5 M m³/year to 440,000 m³/year, the lowest mobilized volume of this scenario, in the reach immediately before the dam. It is worth mentioning that even though the slope is the same in this reach, the transport rate is not the same as the one observed in Scenario III. After the dam, the average mobilized volume was 1,6 M m³/year.

3.5. Comparison between scenarios

Figure 15 displays the mean mobilized volume obtained for each slope scenario across all reaches, accompanied by their respective slopes.

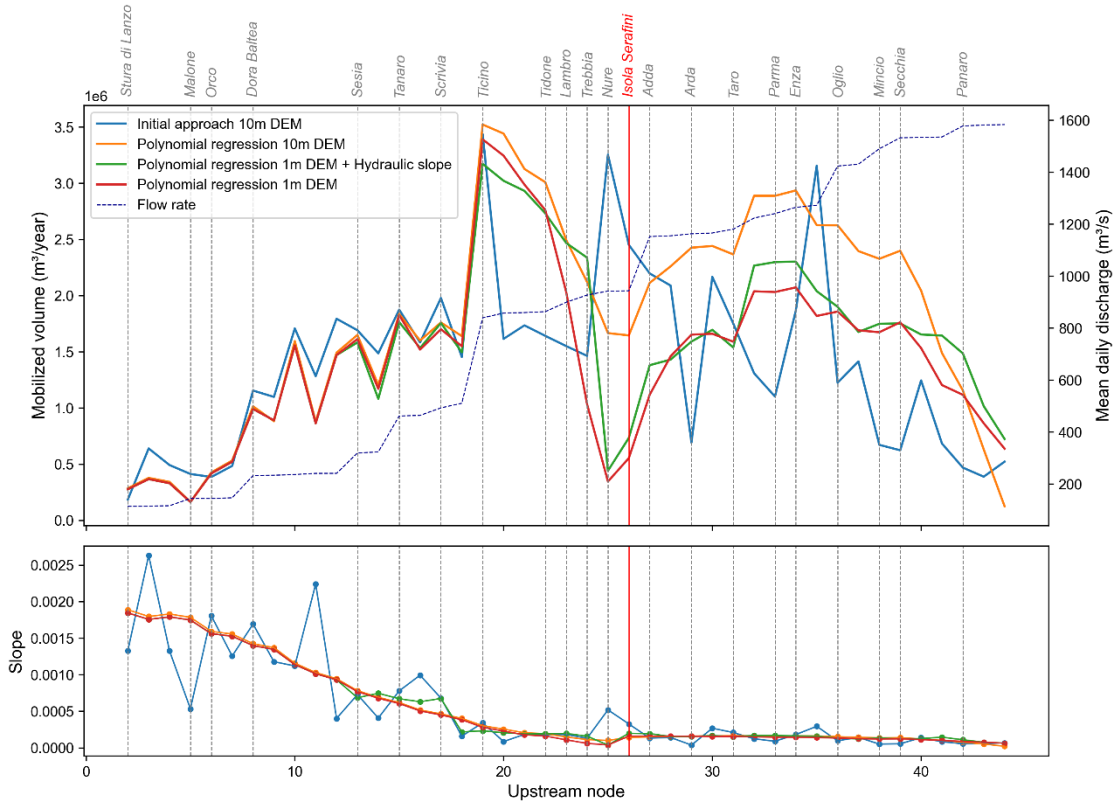

Figure 15. Mean annual mobilized volumes, mean daily flow rate, and the corresponding slopes across all reaches for each scenario.

Scenarios II, III, and IV show a similar trend, varying in magnitude. This variability is virtually insignificant upstream and intensifies downstream. For instance, a 9% variation in slope in Reach 25 resulted in a substantial shift in mobilized volume, from 350,000 m³/year (Scenario III) to 1,6 M m³/year (Scenario II).

Scenario I stands out as the most distinct among the four. However, while the slope of this scenario undergoes significant variation upstream, the disparity in magnitude compared to the other scenarios is relatively minimal, and the overall trend remains similar until Reach 19. Additionally, all slope scenarios featured the same reach with the highest peak of annual mean values (Reach 19).

Figure 16 illustrates the mobilized volume height across all reaches for each scenario. Notably, scenarios I and IV reached the model's maximum mobilization limit (i.e., max. active layer) at the highest peak of discharge. Specifically, in scenarios II to IV, the highest mobilization height occurred in the Reach 21. This reach is situated in a highly dynamic region and has a smaller area compared to its neighboring reaches. The mobilization height in this reach ranged from 17.5 to 30 cm, with the latter constrained by the maximum active layer parameter.

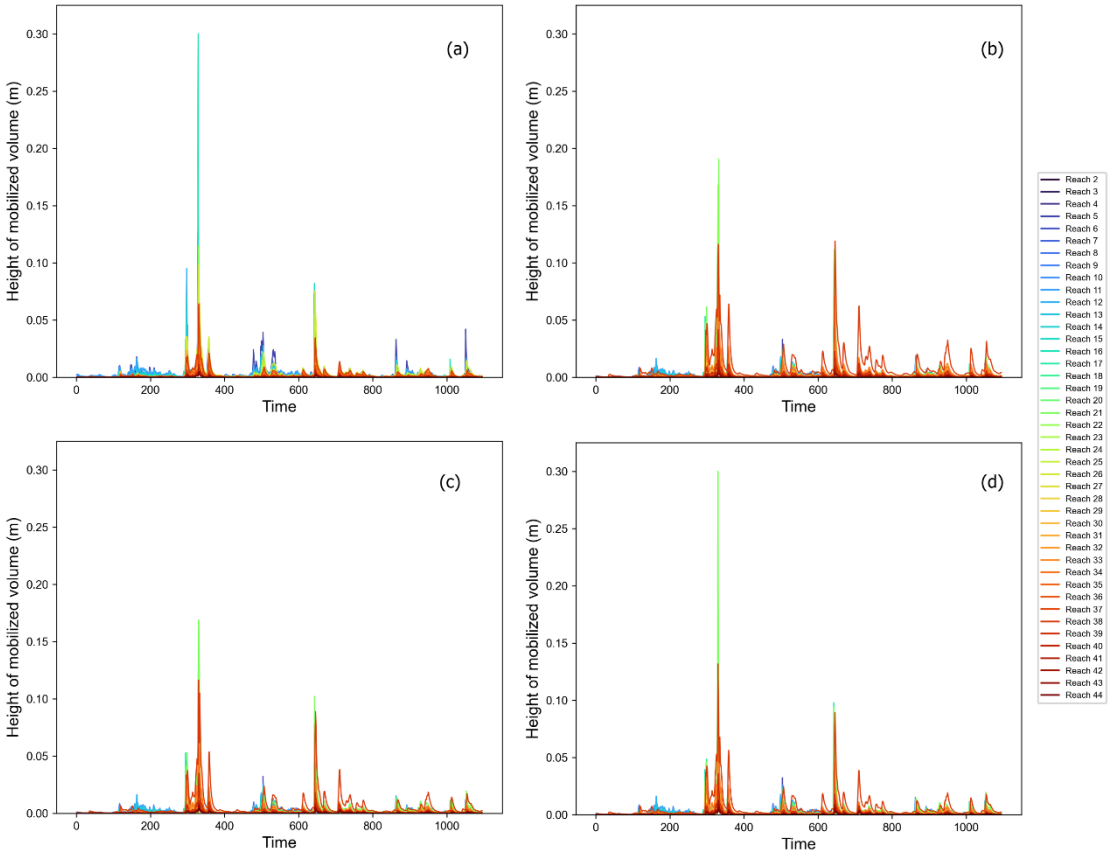

Figure 16. Temporal variation in height of mobilized volume across all reaches for Scenarios I, II, III, and IV (a, b, c, d, respectively).

Figure 17 depicts the temporal evolution of the D50 of the mobilized layer across all reaches for each scenario. This visualization aids in comprehending the grain size distribution of the mobilized volume along the river. Higher D50 values are seen in upstream reaches, particularly in the Reach 5, at the confluence with the Malone tributary. In contrast, the remaining reaches exhibited significantly low D50 values.

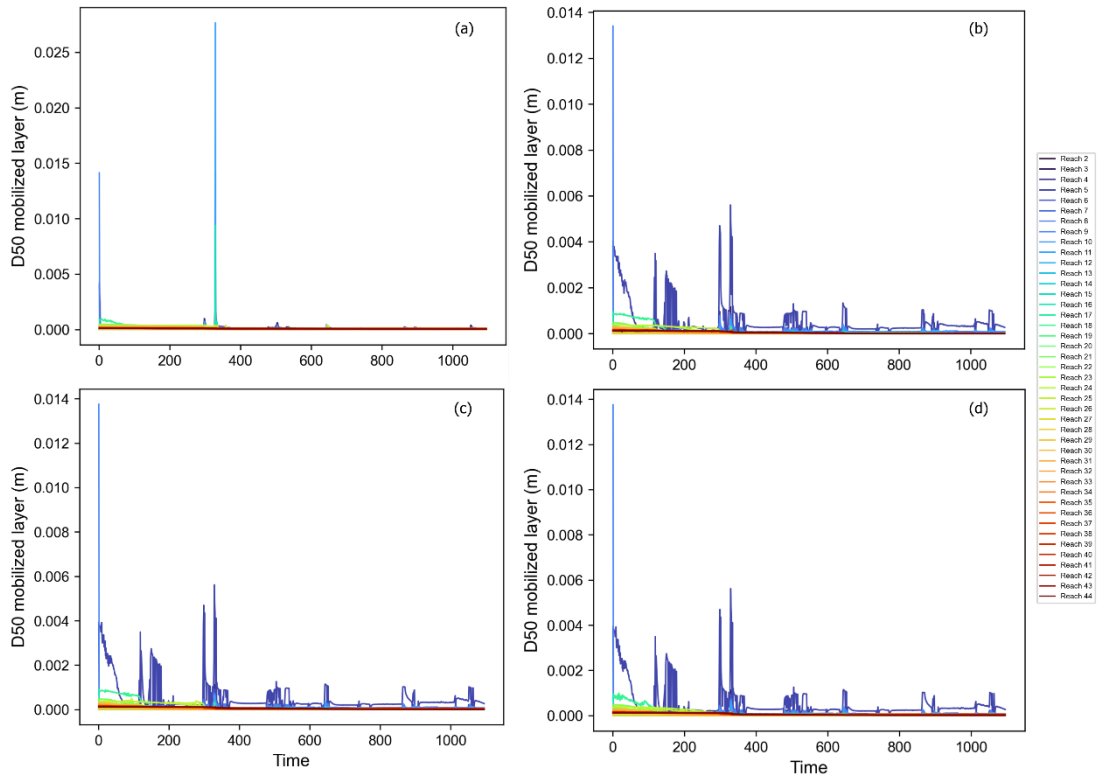

Figure 17. Temporal variation in height of mobilized volume across all reaches for Scenarios I, II, III, and IV (a, b, c, d, respectively).

3.5.1. Comparative analysis of Scenarios II and III: Reaches 25 and 26

As previously mentioned, both Scenarios II and III have led to certain reaches exhibiting higher bed material fluxes during the flood peak of 2020 compared to the peak of 2019, despite the latter being larger than the former. To conduct a comparative analysis between these scenarios, Figures 18 and 20 illustrate the temporal evolution of discharge, mobilized volumes, and deposited volumes for Reach 25 and Reach 26 in Scenarios II and III, respectively. Additionally, Figures 19 and 21 provide a comparison of transport capacity and mobilized volumes over time for these reaches in both scenarios.

To understand this phenomenon, it is crucial to analyze the distribution of sediment volume along the river in the preceding year within each scenario. In Scenario II, as depicted in Figure 18, Reach 25 emerges as a significant depositional site, accumulating a substantial sediment load from upstream during the highest flood peak in 2019.

Although Reach 26 also receives sediment, its volume is one order of magnitude smaller than that of Reach 25. As shown in Figure 17, the mobilized sediments mainly consist of finer particles, underscoring their significance according to the Engelund-Hansen formula.

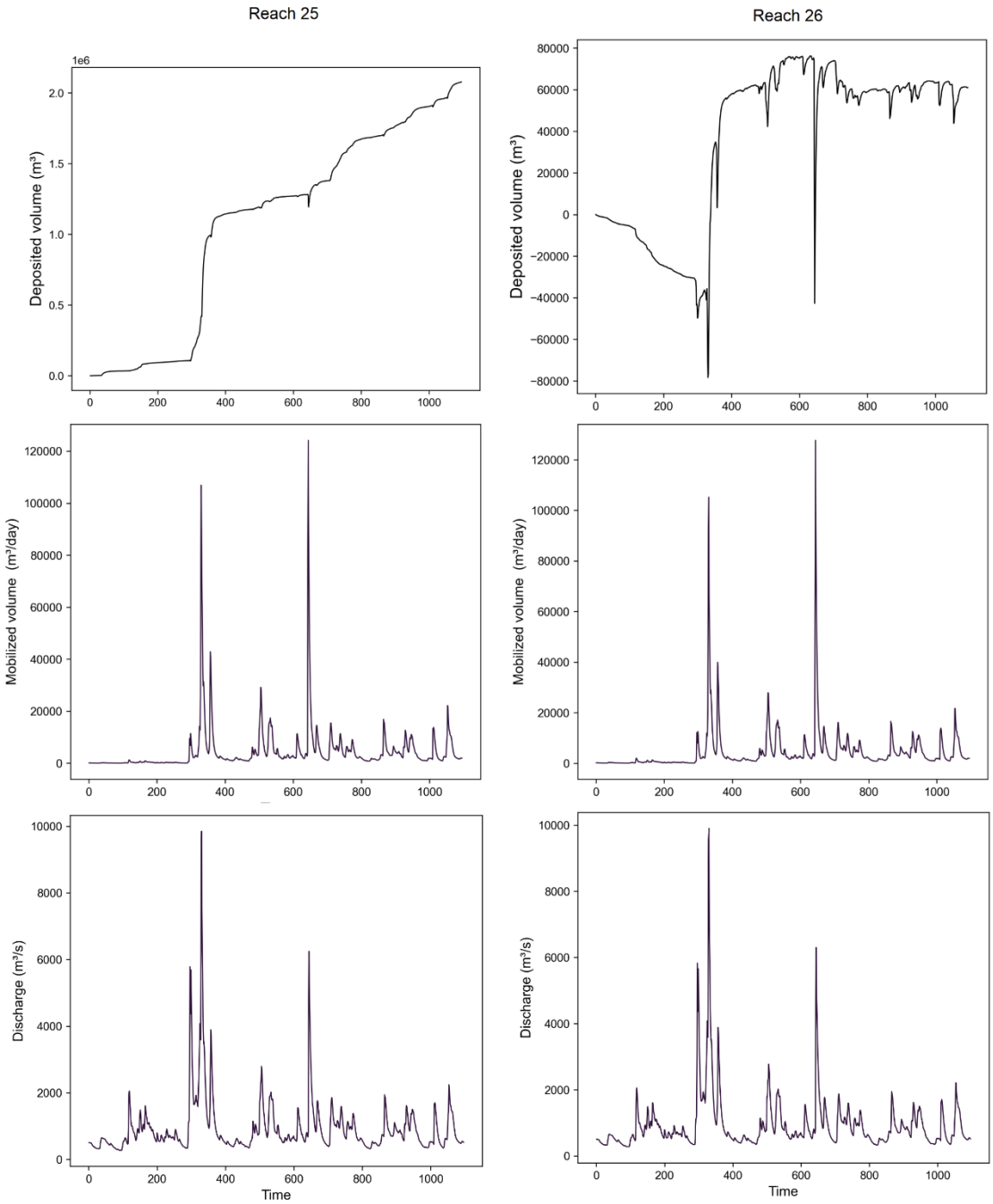

Figure 18. Temporal evolution of deposited and mobilized volume in Reaches 25 and 26, depicted for Scenario II (Polynomial regression using 10m DEM).

Continuing the analysis of Scenario II, Figure 19 reveals that Reach 25 exhibited a higher transport capacity during the discharge peak in 2020, which can be attributed to the deposition of finer sediments following the initial flood event. This is related to the fact that these finer sediments are easier to be transported. In contrast, during the first peak, Reach 26 directed its available energy towards a sediment class in starvation, resulting in a mobilized volume lower than its transport capacity. However, during the second peak, similar to Reach 25, the presence of finer deposited sediments increased transport capacity due to its dependency on grain size.

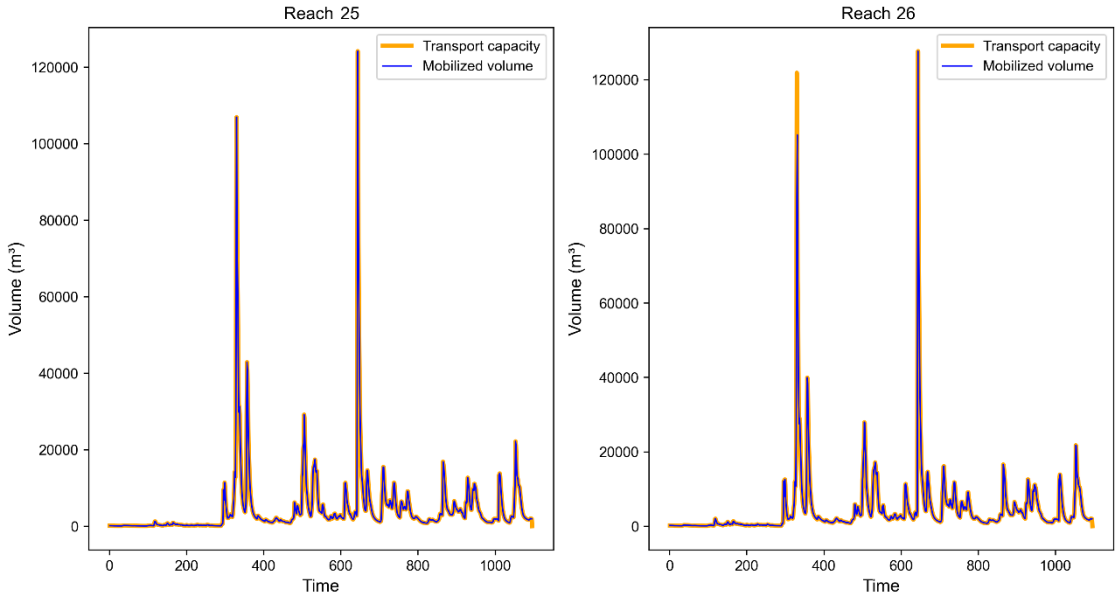

Figure 19. Temporal evolution of transport capacity and mobilized volume Reaches 25 and 26, depicted for Scenario II (Polynomial regression using 10m DEM).

In contrast, in Scenario III Reach 26 consistently experiences erosion, indicating a lack of sediment deposition from upstream sources (Figure 20). Consequently, as shown in Figure 21, it exhibited a higher transport capacity during the flood peak in 2019 compared to 2020 due to the presence of a larger volume of finer sediments, which were carried away after the initial peak and not replenished.

Reach 25 also demonstrated itself as a significant depositional site in Scenario III, accumulating more deposited volume by the end of the simulation than in Scenario II (Figures 18 and 20). Although it displayed a similar pattern regarding differences in

mobilized volumes between the two flood peaks, the bed material fluxes in Scenario III were notably reduced. As depicted in Figures 18 and 21, Reach 25 demonstrates a consistent behavior across both scenarios, with transport capacity equating to mobilized volume.

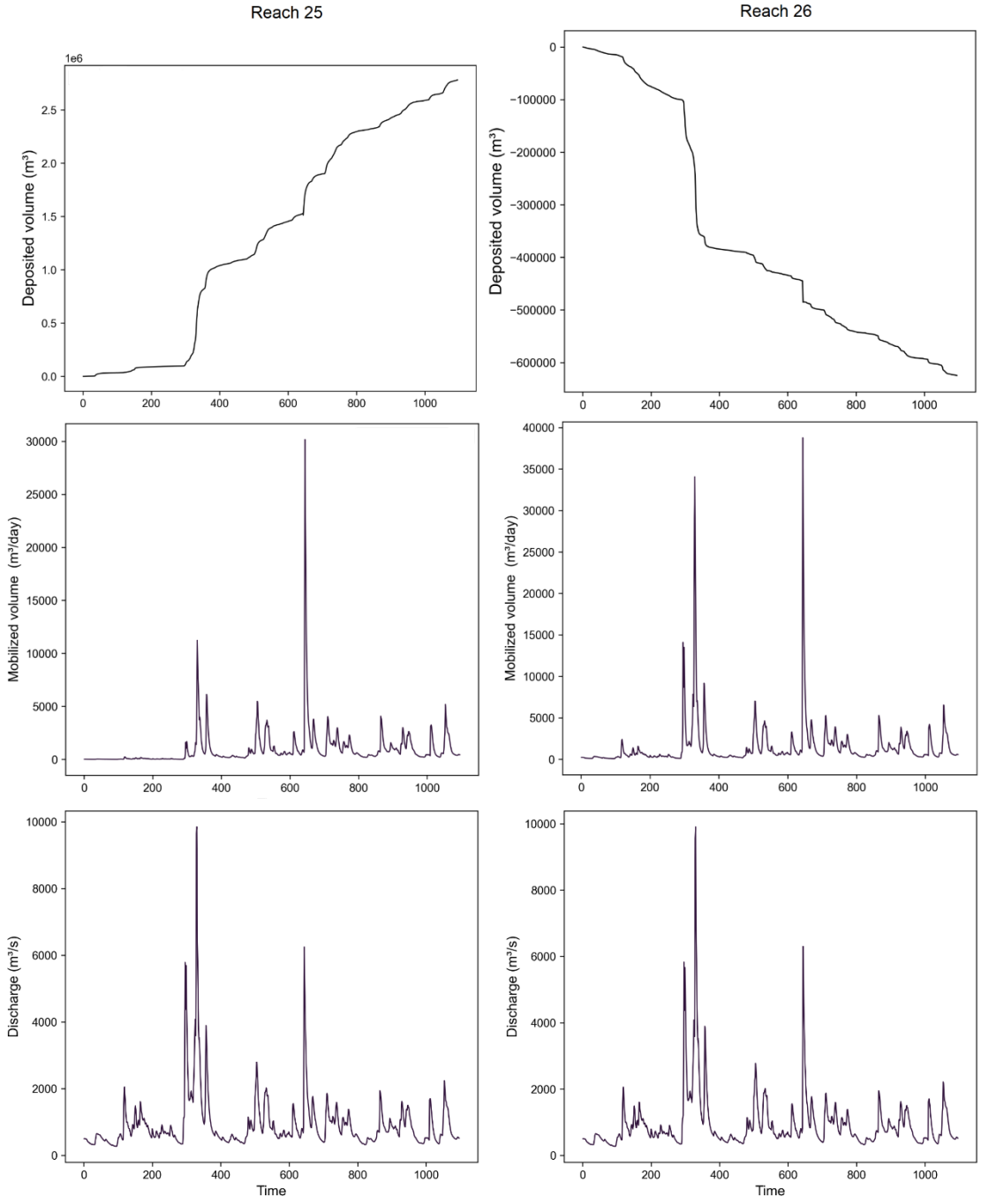

Figure 20. Temporal evolution of deposited and mobilized volume in Reaches 25 and 26, depicted for Scenario III (Polynomial regression using 1m DEM).

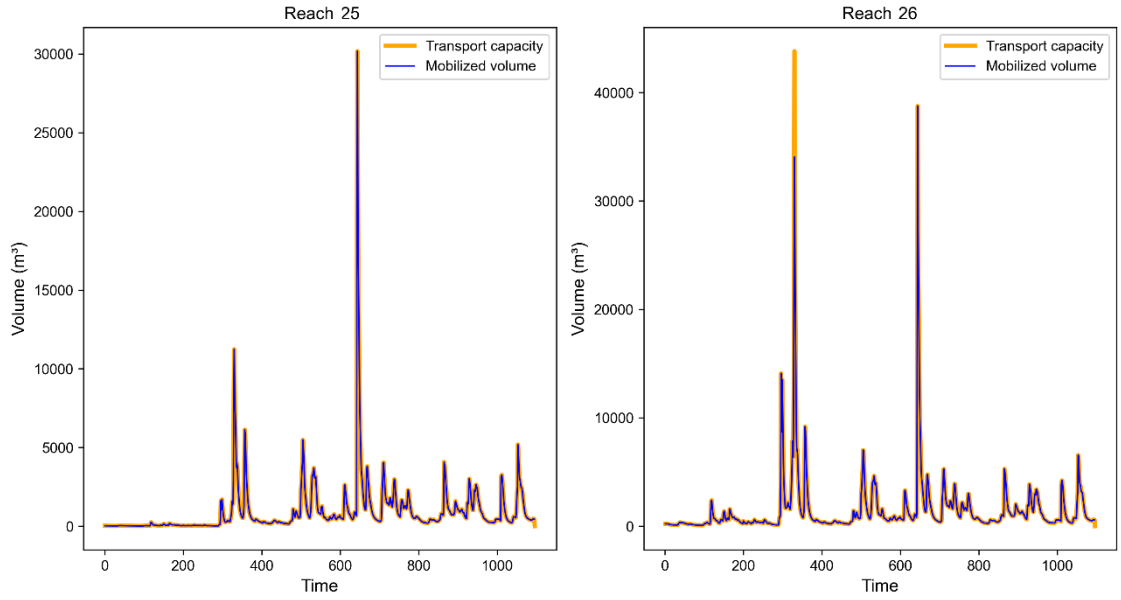

Figure 21. Temporal evolution of transport capacity and mobilized volume in Reaches 25 and 26, depicted for Scenario III (Polynomial regression using 1m DEM).

3.6. Validation

3.6.1. Site-specific observations

Table 4 displays the observed bedload transport rates and the simulated sediment fluxes found for each slope scenario.

Table 4. Comparison between observed and simulated bedload sediment fluxes for each slope scenario.

Slope scenario	***Observed and simulated discharge (m³/s)***	***Observed sediment flux (g/s/m)***	***Simulated sediment flux (g/s/m)***
Initial approach 10m DEM	1300 – 1800	4 – 26	4 – 21
Polynomial reg. 10m DEM			11 – 63
Polynomial reg. 1m DEM			9 – 34
Poynomial reg. 1m DEM + Hydraulic slope			12 – 39

The sampling performed by Schippa et al. (2021) displayed a total sediment flux ranging from 4 to 26 g/s/m, with the highest bedload transport rate verified for the lowest discharge (1300 m^3/s). The simulated sediment fluxes for all four slope scenarios were in the same order of magnitude of the observed values and fell within the same variability window of the observations, ranging from 4 to 63 g/s/m.

3.6.2. Sediment management plan

Figure 22 compares the simulated mean annual mobilized volumes for each slope scenario with the mean annual budget of bed material flux obtained from the Po River sediment management plan (PGS). The PGS considers the average sediment budget for the period between 1982 and 2005.

It was noticed that Scenario I presents an unrealistic portrayal of mobilized volumes, featuring peaks often followed by troughs, suggesting significant fluctuations in mobilized volume per reach, even within successive reaches. Conversely, Scenarios II to IV exhibit a trend similar to that indicated by the PGS, albeit varying in magnitude. The average bedload transport value, observed after Tratto C, stands at 4,5 M m^3/year, exceeding the range of average simulated sediment flux, which falls between 1,5 to 2,5 M m^3/year.

Firstly, both Tratto A and Tratto B (between Stura di Lanzo and Ticino) exhibit a consistent increase in mobilization, mirroring the trends observed in the validation data. At the Ticino confluence, there is a notable sharp rise in mobilization, although the magnitude differs slightly from the validation scenarios.

In contrast, Tratto C, situated between the Ticino and Trebbia rivers, displays no significant increase in mobilization in the results, contrary to the predictions made by the PGS. The presence of the Isola Serafini dam (Tratto D) corresponds to a decrease in mobilization, consistent with both the reference and our findings. This decline is attributed not only to the dam but also to navigation and material extraction activities in the area.

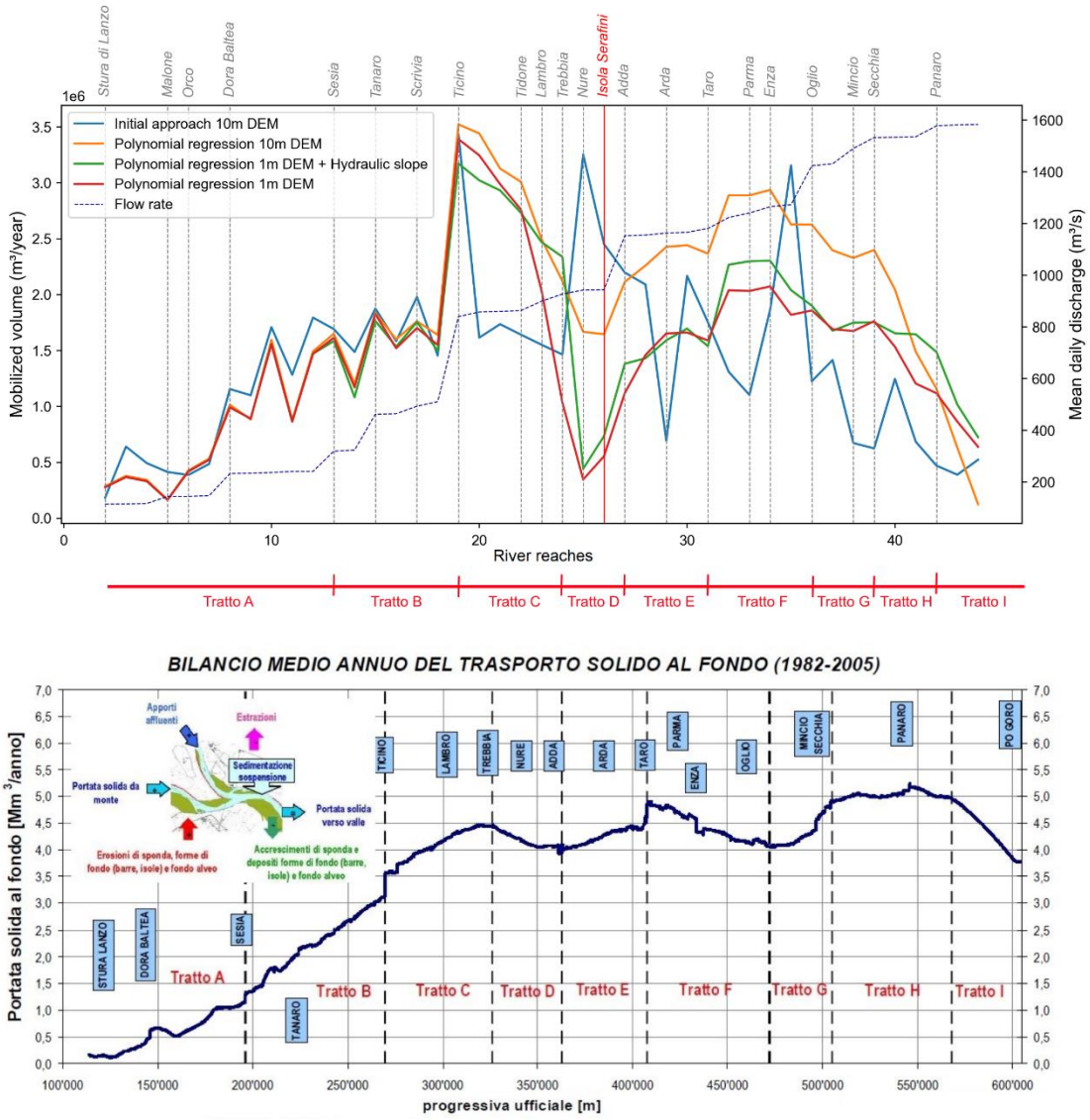

Figure 22. Comparison between simulated mobilized volume for each slope scenario and the mean annual budget from the Po River sediment management plan.

Moving along the river, an increase in mobilization is observed between the Adda and Taro rivers (Tratto E), aligning with the trends identified in the validation data. Tratto F, downstream from Taro, experiences a surge in mobilization due to contributions from the Taro River and external sediment sources, influenced by lateral connectivity. Subsequently, mobilization begins to decline, a trend also reflected in the results.

Tratto G, covering reaches between upstream nodes 36 and 40, diverges from the validation data, showing an increase in mobilization instead of the expected decrease. This discrepancy may be attributed to various factors not captured by the model. Beyond

the Panaro River, a significant decrease in bedload transport occurs as the river meets the sea, a trend consistent with both the reference model and our findings, albeit on a larger scale in the obtained results.

CHAPTER 4

4. DISCUSSIONS

4.1. Slope scenarios and sediment connectivity

Elevated discharge rates are associated with increased transport capacity, yet the actual mobilized volume also relies on sediment availability within specific grain size classes in the reaches (Church, 2006). This availability is significantly shaped by the slope gradients along the river network. The Reaches 25 and 26 are located immediately before and after the dam, providing a crucial section to gain insights into how the slope scenarios portray sediment connectivity, despite not accounting for sediment trapping caused by the dam. As mentioned in the results section, Figures 18 and 20 demonstrate that in Scenario II, deposition still occurs in reach 26, positioned just after the dam, while in Scenario III, only erosion is observed.

Figure 15 highlights that the slopes in scenarios II and III exhibit overall similarity, though they show more pronounced differences as they approach the Isola Serafini dam. These discrepancies occurred due to differences in elevation data between the two DEMs used for slope extraction, which can be attributed to disparities in terms of spatiotemporal resolution. As already mentioned in the data and methods section, the 10-meter resolution DEM consists of bare ground elevation data from 2005, while the LiDAR-derived DEM with a 1-meter resolution collected in 2021 provides surface elevation data, likely incorporating water slope, which is crucial for accurately assessing transport capacity.

Furthermore, geomorphological conditions may have undergone changes over the 16-year period between 2005 and 2021, as indicated in several studies discussing the dynamic nature of the Po River (Brenna et al., 2022, 2024; Surian & Rinaldi, 2003). These changes could entail alterations in reach width, elevation, and slope, particularly in the vicinity of the Isola Serafini dam, which underwent modifications including the addition of a new navigation lock in 2018. It is worth mentioning that the necessity for this modification arose from the lowering of the riverbed, rendering the previous lock unusable.

Notably, the DEM with a 10-meter resolution presents a 4-meter elevation difference before and after the dam, whereas the one with a 1-meter resolution shows a sudden decrease of 9 meters in elevation. This results in differing slope patterns between the two scenarios, contributing to increased sediment disconnectivity with higher-resolution input data. These observations align with findings from Lisenby & Fryirs (2017), who concluded that, for their approach and scale of study, employing a finer-resolution DEM resulted in disconnections within the river network. In this study, the Isola Serafini dam plays an important role in sediment connectivity (Bizzi et al., 2015), and obtaining more detailed elevation data in this region was deemed valuable for assessing sediment fluxes.

4.2. Slope and DEM resolution

Schoorl et al. (2000) stated that coarser resolutions tend to result in higher erosion rates compared to finer resolutions, a trend corroborated by the results from Scenarios I and II, showing higher mobilized values compared to Scenarios III and IV (Figure 15). Another important observation is that the mobilized outcomes of the model are more sensitive to changes in slope downstream. This sensitivity arises from the higher values of discharge downstream, resulting in greater variability of mobilized volume despite smaller differences in slope. This aspect is important to consider during slope extraction because it suggests that even minor variations resulting from errors or inaccuracies in slope retrieval could lead to unrealistic spikes in the results in reaches with high flow rates. In this context, Scenario I, which relies on data obtained from single pixels (nodes upstream and downstream) subjectively chosen by the operator, is more susceptible to such errors.

However, it was observed that the method of slope extraction could help alleviate some errors associated with coarser resolutions. This is evident from the significant disparities between Scenarios I and II, despite originating from the same data source. Employing regressions can further mitigate errors associated with point elevation samples, although it is essential to acknowledge that their implementation inherently involves smoothing the topographic data.

4.3. Validation of simulated sediment fluxes

From the site-specific validation (Table 4), it was observed that the simulated sediment fluxes across all four slope scenarios generally aligned with the observed values, falling within a comparable range of variability. However, the findings from Schippa et al. (2021) unveiled a highly variable and nonlinear relationship between total sediment flux and water discharge. To ensure a comprehensive validation of the results, it is crucial to have spatially distributed validation data, enabling a thorough assessment of whether the simulated network accurately responds to observed sediment sources and sinks.

Comparing the scenarios with the sediment management plan (PGS) (Figure 22), it becomes evident that while Scenarios II, III, and IV generally demonstrate similar trends to the PGS, there are notable differences in magnitude. These disparities may arise from various limitations within the simulation process, such as uncertainties regarding the sources and quantities of sediment routed in the model. This encompasses the volume of material initialized in the reaches, directly linked to contributions from tributaries, as well as the absence of external sediment contributions to replicate sediment delivery from hillslopes.

Moreover, adopting a constant width value for the reaches (active channel width), regardless of discharge variations, could potentially lead to an underestimation of the mobilized volume during periods of lower discharge. Furthermore, using mean daily discharge for simulations may result in reductions in total sediment loads due to the nonlinear response of sediment transport to fluctuations in water discharge at a daily scale. Nonetheless, this choice is considered the most sensible for the daily sediment flux simulations conducted by D-CASCADE.

Regarding the differences in trends between results and PGS, a steeper descent in sediment fluxes was observed in the latter part of the river compared to the PGS. This inconsistency could be attributed to the simulation focusing solely on bed material from sand to larger fractions, whereas the total load in this river section may primarily consist of silt and clay, which is not ideal to be represented by the Engelund-Hansen (EH) sediment transport formula. This observation is supported by the findings of Ma et al. (2017), which noted an abrupt transition in the sediment transport regime around the sand-silt threshold, leading to an underestimation of bed material load by the EH formula.

However, it is essential to acknowledge the uncertainties associated with the PGS evaluation, which may also contain inaccuracies. As mentioned in the data and methods

section, the assessment combines morphological evidences with transport capacity calculations, assuming a transport-limited hypothesis with full supply, thereby introducing its own set of limitations. Therefore, more field evidence and measurements of sediment transport in the lower reach of the Po River are necessary to determine whether sediment transport is indeed decreasing and for which sediment fraction.

Overall, evaluating the accuracy of sediment transport modeling poses challenges due to the limited availability of sediment transport data, which are frequently characterized by high variability and uncertainty even when available. Therefore, having simulation results that fall within a similar order of magnitude or within the same range of variability as observed data can be considered satisfactory given the inherent uncertainties in both observations and model inputs.

4.4. Understanding modeling uncertainties

According to Tangi et al. (2022), simulating complex processes over large spatial and temporal scales can generate diverse uncertainties, including those arising from boundary conditions and modeling parameters. Investigating numerous hypotheses and scenarios is crucial to adequately manage these uncertainties.

During the modeling process, several simplifications were adopted, all of which require careful consideration. Many of these simplifications could be addressed with the availability of field evidence at a network scale, particularly regarding grain size sampling at the tributaries and their contributions to the Po River.

One notable concern is the potential for temporal inconsistencies resulting from the use of grain size data from 2005 alongside discharge data spanning from 2018 to 2021. Given the possibility of geomorphological changes occurring between these periods, these two datasets may not be compatible. Additionally, the absence of tributary grain size data forced the assumption that it matches that of downstream reaches in the Po River network. Uncertainty also arises from model parameters, such as the maximum active layer and the initial deposited volume per meter length within the reaches, which are assumed to be uniform across all reaches.

Another source of uncertainty arises from the integration of slopes obtained from different data sources in Scenario IV, which incorporates slopes from both the 1-meter

resolution DEM and hydraulic simulations. This combination led to slope discontinuities, as observed in Reach 25 (Figure 14), where abrupt changes in mobilized volume occur. Therefore, having modeled hydraulic slopes for the entire river network would be advantageous in this regard.

Despite the uncertainties related to the model inputs, D-CASCADE offers a flexible modeling platform that users can employ for their river networks. This tool should be seen as an exploratory resource, allowing users to test various input combinations, including different sediment transport formulas, to ensure alignment with observed patterns and anticipated behaviors (Tangi et al., 2022). Users retain the freedom to refine input data and explore alternative methodologies tailored to their specific needs, whether focused on analyzing annual sediment budgets or investigating sediment provenance.

4.5. Sediment fluxes and discharge variability

Discharge variability, influenced by climatic events like snowmelt and extreme precipitation, significantly impacts yearly sediment fluxes. Higher discharge during such events increases sediment transport rates due to greater water flow erosive power. Analysis of the results for each scenario shows significant changes in yearly sediment transport rates corresponding to discharge fluctuations (Figure 12).

In 2019, a notably higher peak, attributed to a flood event documented by Pavan et al. (2020), resulted in increased sediment transport across most of the reaches in each of the slope scenarios. For example, in Reach 19, a variability of approximately 40% in the annual mean daily discharge (from 713 m^3/s in 2021 to 980 m^3/s in 2019) led to an increase of around 60% in the total mobilized volume per year (from 2,5 Mm^3 in 2021 to 4 Mm^3 in 2019) across all four scenarios (Figures 10, 11, 13 and 14). Moreover, this underscores the non-linear response of sediment transport to an increase in water discharge.

4.6. Challenges and future directions

During this study, employing point samples of elevation from the 10-meter resolution DEM resulted in unrealistic sediment mobilization outcomes, particularly evident in

Scenario I. Consequently, a polynomial regression was applied to the Po River elevation profile, revealing shifts in the slope primarily attributed to the presence of dams, with the Isola Serafini dam being the most significant. Segmentation of elevation data was necessary to achieve a satisfactory fit, highlighting a notable challenge in modeling large-scale rivers. While the Po River features a single major dam, other rivers, particularly in Europe where barriers are prevalent (Belletti et al., 2020), may require more extensive efforts to model the elevation data accurately.

One of the critical challenges lies in adequately parameterizing the model to account for the heterogeneity of landscapes and spatial variations in geomorphic processes (Tangi et al., 2022a). Essential to achieving this objective is the acquisition of reliable datasets for model calibration and validation, a process often demanding extensive field observations and monitoring, which may not always be readily accessible (Temme et al., 2013). Throughout this study, acknowledging these challenges highlighted the need for more site-specific field evidence to establish realistic thresholds and account for inherent uncertainties through sensitivity analyses.

Furthermore, sediment transport relationships are inherently imperfect and may not accurately correspond to other datasets when tailored to fit one group (Temme et al., 2013). Choosing a representative formula for sediment flux modeling at a river network scale poses another challenge, given the transitions of grain size distribution along the river, from coarser sediments upstream to finer sediments downstream.

As depicted in the comparison of the scenarios (Figure 15), the trends in mobilized volume exhibit similarity across three of the four scenarios, despite variations in magnitude. This suggests a level of consistency in the underlying processes, regardless of the specific method employed for slope computation. It is noteworthy to acknowledge that while there are multiple approaches to generating slope, each method comes with its own set of limitations. Determining the optimal approach depends on several factors, including the scale of the investigation and the availability and quality of data, particularly in terms of spatiotemporal resolution.

Another interesting observation emerges when comparing Scenarios III and IV (Figures 15). In Scenario IV, alongside some upstream and downstream reaches, Reach 25, positioned within the middle section of the Po River, was supplemented with a slope from Scenario III. Although the slope was the same in this reach, there were differences

in the simulated mobilized values across the scenarios. This variance can be attributed to the slope gradient composed by the upstream reaches, which also impacts sediment mobilization in Reach 25, beyond its own slope. Slope gradients determine the pathways along which sediment moves within the river network and significantly influence the composition and volume of materials reaching Reach 25. This emphasizes the importance of understanding sediment dynamics at a network scale to comprehend localized processes thoroughly.

Furthermore, considering the implications of these findings, future studies may benefit from exploring the robustness and scalability of different methods to obtain slope across diverse river networks. Incorporating sensitivity analyses to assess the impact of varying methodological choices on model outcomes could provide valuable insights into the reliability and applicability of these approaches in different contexts. Ultimately, advancing our understanding of slope computation methodologies contributes to refining river network modeling techniques and enhancing our ability to accurately characterize sediment transport dynamics at broader spatial scales.

CHAPTER 5

5. CONCLUSIONS

This study explored how different slope scenarios affect the modeling of bed material fluxes in the Po River basin. The mobilized volume results were validated using both site-specific and network-scale datasets. The findings offer insights into the differences and similarities arising from different elevation data inputs and slope computation methods. Additionally, the study discusses challenges encountered during the investigation and suggests directions for future research.

When considering methods for deriving slope from Digital Elevation Models (DEMs), a first approach using punctual elevation samples for the slope computation resulted in unrealistic spikes of mobilization, probably due to the higher susceptibility to errors associated with this approach. Conversely, employing a polynomial regression, considering shifts in elevation along the river profile due to structural elements, was demonstrated to reduce the influence of these errors.

The utilization of a coarser resolution DEM for slope computation resulted in overall higher values of mobilized volumes. In addition, a more recent and detailed DEM led to an increased sediment disconnectivity around the Isola Serafini dam, notwithstanding the absence of sediment trapping considerations. This could be related to more detailed topographic information in this region or even to geomorphological changes between the two DEMs. Furthermore, the findings suggest that slope is an especially sensitive parameter for lowland reaches, where higher values of discharge are observed.

A site-specific measurement was used to validate sediment fluxes for given discharge values in a specific reach. The simulated sediment fluxes for all scenarios fell within the same order of magnitude and range of variability as the observed ones. However, this field evidence showed a highly non-linear relation between discharge and bed material fluxes. This underlines the importance of other field measurements for validation.

Out of the four scenarios tested, three exhibited similar trends with varying magnitudes. Upon comparing these simulated trends to the average annual sediment fluxes provided by the sediment management plan, similar patterns were noticed, albeit with lower magnitudes in the simulations. This divergence could be attributed to

uncertainties in the model inputs and limitations of the Engelund Hansen formula in representing the entire scale of the Po River basin, given the variations in grain size distribution. Nevertheless, considering the uncertainties associated with both assessments, the observed similarities were deemed satisfactory.

Additionally, the results highlight the significant influence of discharge variability on yearly mobilized volumes and underscore the nonlinear relationship between sediment transport and discharge variability.

The D-CASCADE model has proven to be a useful tool in simulating sediment fluxes at a river network scale due to its flexibility and scalability. It requires limited computational resources, making it possible to simulate models quickly and repeatedly, allowing for the investigation of different scenarios. However, more spatially distributed evidence of sediment transport across the Po River basin is necessary to appropriately calibrate and validate the model. Sensitivity analyses may help to account for intrinsic uncertainties, which would improve the reliability and accuracy of the simulations. Ultimately, this would contribute to better sediment management practices in the region.

ACKNOWLEDGEMENTS

I would like to express my sincere appreciation to my supervisor, Prof. Simone Bizzi, for his support, expert guidance, and insightful feedback, which have been instrumental in shaping this thesis. I also extend my heartfelt thanks to the entire research group for their invaluable contributions, encouragement, and collaborative spirit throughout this journey. I am sincerely thankful for the chance to collaborate with such outstanding researchers.

APPENDIX

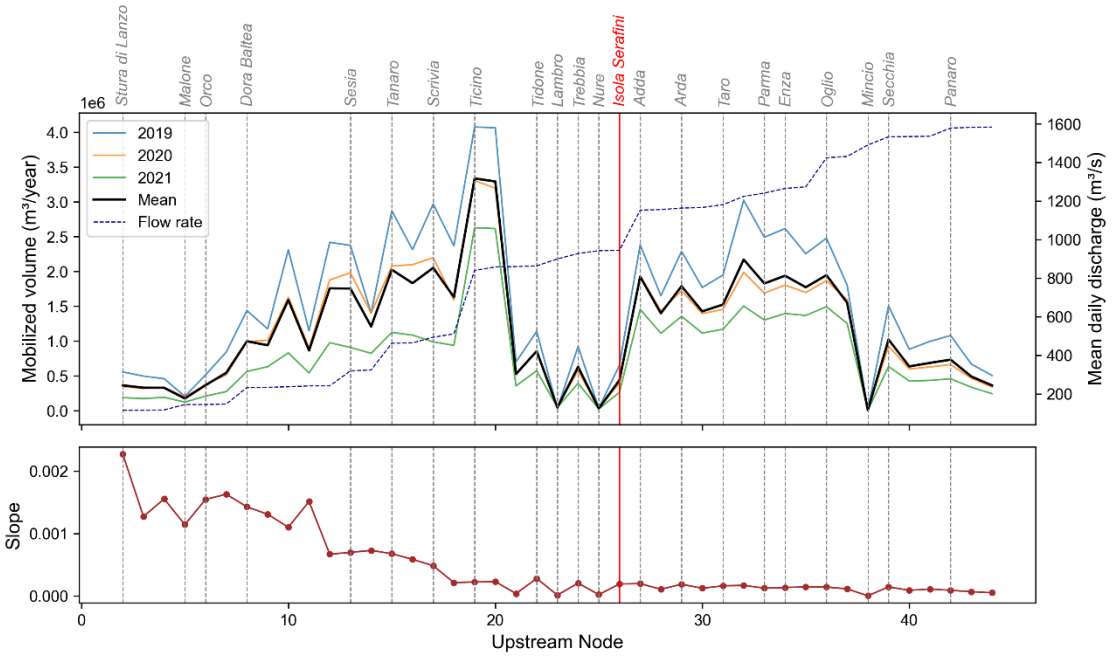

Figure 23. Mean annual mobilized volume, mobilized volume per year, mean daily flow rate, and the corresponding slopes across all reaches. Slope computation method: elevation differences between upstream and downstream nodes, sampled from the 1-meter DEM.

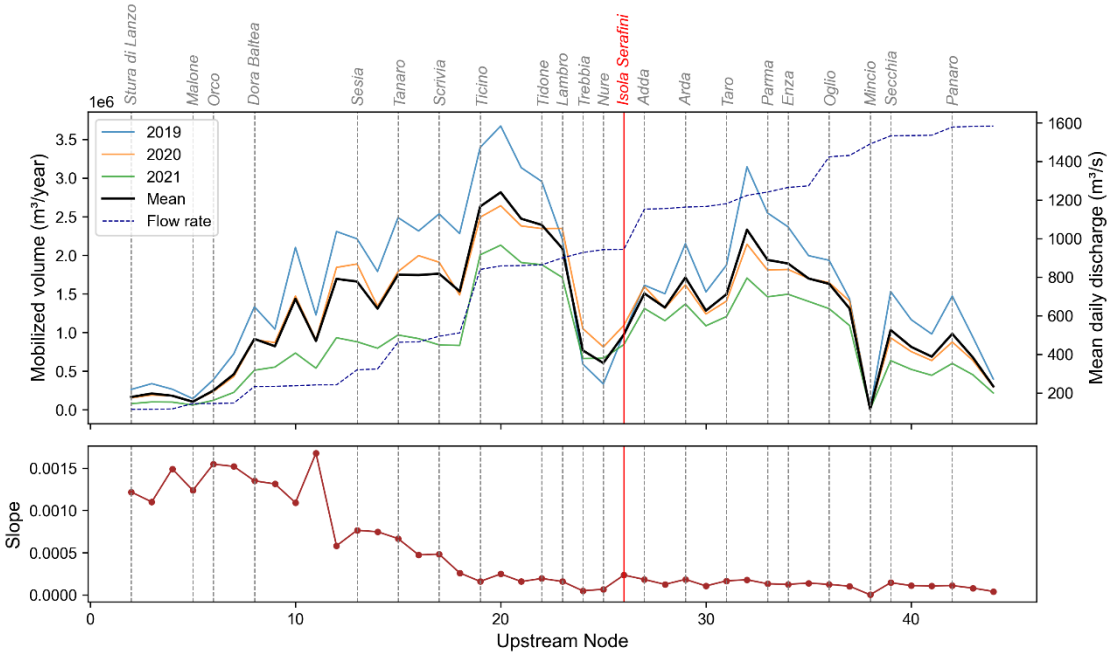

Figure 24. Mean annual mobilized volume, mobilized volume per year, mean daily flow

rate, and the corresponding slopes across all reaches. Slope computation method: linear regressions on a per-reach basis, utilizing elevation data from the 1-meter DEM.

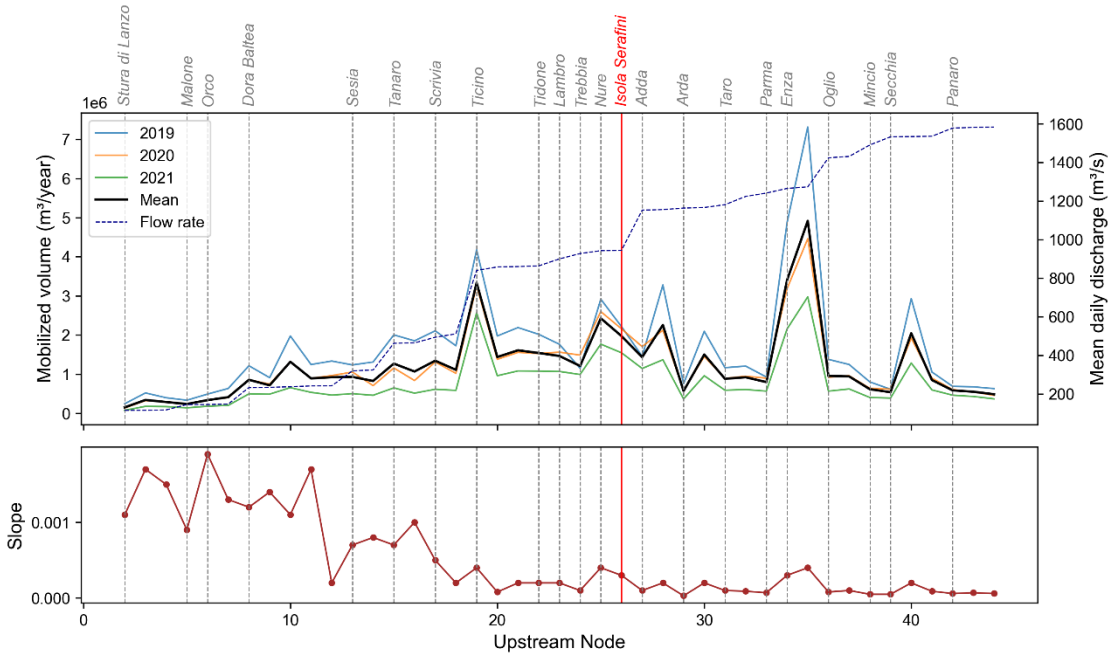

Figure 25. Mean annual mobilized volume, mobilized volume per year, mean daily flow rate, and the corresponding slopes across all reaches. Slope computation method: linear regressions on a per-reach basis, utilizing elevation data from the 10-meter DEM.

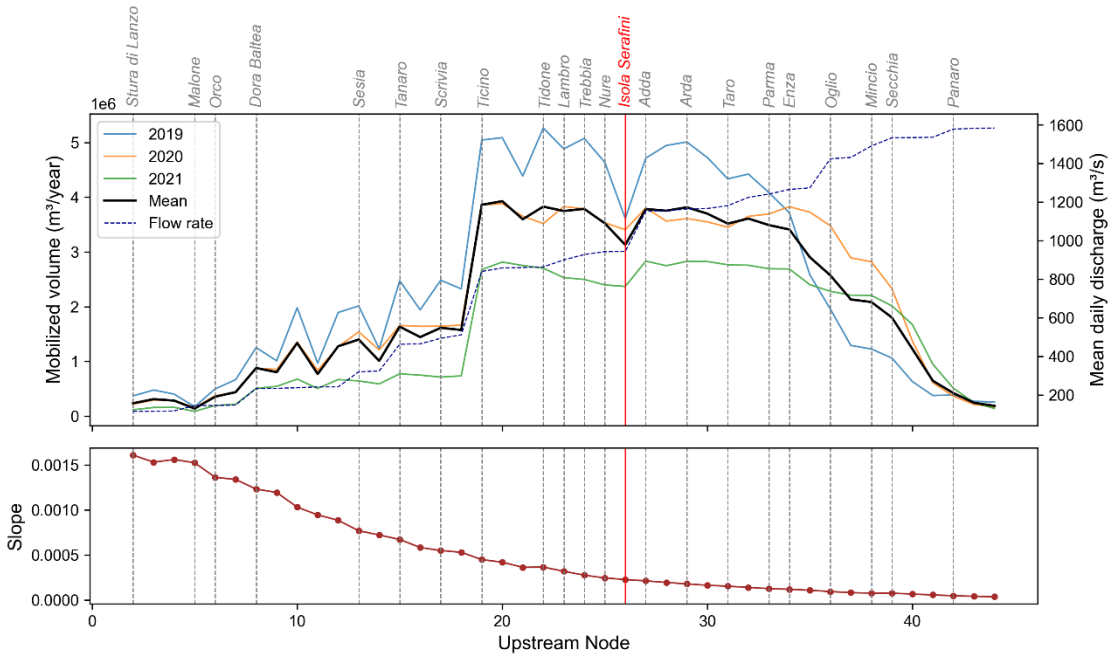

Figure 26. Mean annual mobilized volume, mobilized volume per year, mean daily flow rate, and the corresponding slopes across all reaches. Slope computation method: exponential regression applied on the entire river profile extracted from the 10-meter

DEM.

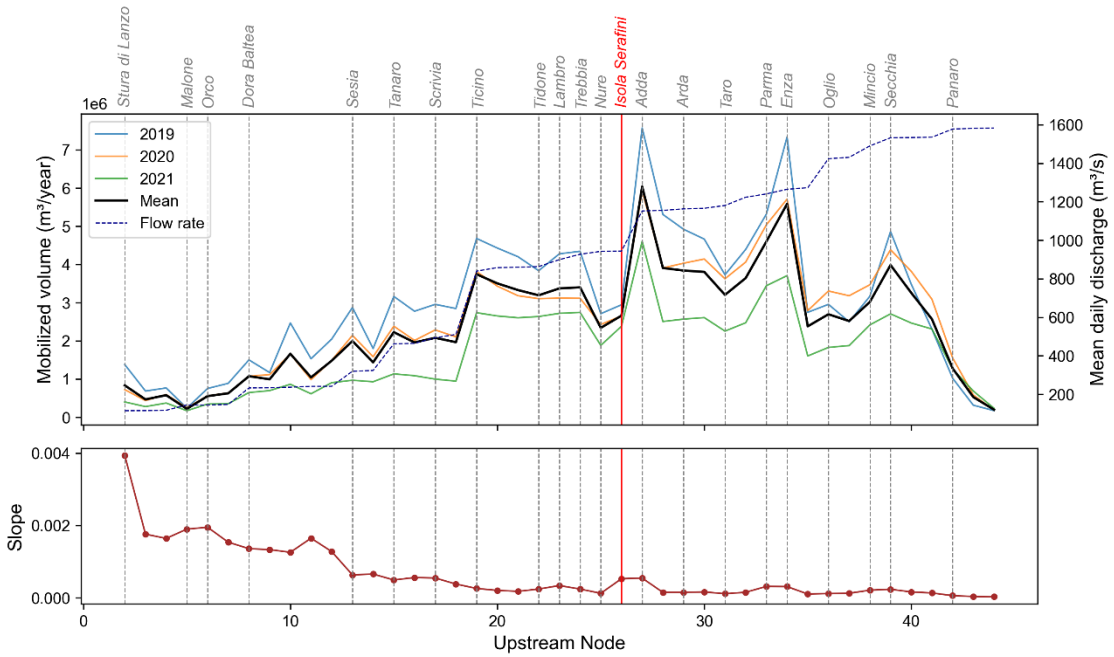

Figure 27. Mean annual mobilized volume, mobilized volume per year, mean daily flow rate, and the corresponding slopes across all reaches. Slope computation: weighted average of river bed elevations derived from cross-sectional elevation data provided by the Interregional Agency for the Po River (AIPO).

REFERENCES

Autorità di bacino distrettuale del fiume Po (AdbPo), 2022. Rinaturazione dell'area del Po, PNRR M2C4 investimento 3.3. Programma d'Azione. In Italian.

Autorità di bacino del fiume Po (AdbPo), 2008, Il recupero morfologico ed ambientale del fiume 574 Po: Il contributo del Programma generale di gestione dei sedimenti del fiume Po. Diabasis, 575 Reggio Emilia, Italy. ISBN 978-88-8103-561-8. In Italian.

Belletti, B., Garcia De Leaniz, C., Jones, J., Bizzi, S., Börger, L., Segura, G., Castelletti, A., Van De Bund, W., Aarestrup, K., Barry, J., Belka, K., Berkhuysen, A., Birnie-Gauvin, K., Bussettini, M., Carolli, M., Consuegra, S., Dopico, E., Feierfeil, T., Fernández, S., … Zalewski, M. (2020). More than one million barriers fragment Europe's rivers. *Nature*, *588*(7838), 436–441. https://doi.org/10.1038/s41586-020-3005-2

Bizzi, S., Dinh, Q., Bernardi, D., Denaro, S., Schippa, L., & Soncini-Sessa, R. (2015). On the control of riverbed incision induced by run-of-river power plant. *Water Resources Research*, *51*(7), 5023–5040. https://doi.org/10.1002/2014WR016237

Bizzi, S., Tangi, M., Schmitt, R. J. P., Pitlick, J., Piégay, H., & Castelletti, A. F. (2021). Sediment transport at the network scale and its link to channel morphology in the braided Vjosa River system. *Earth Surface Processes and Landforms*, *46*(14), 2946–2962. https://doi.org/10.1002/esp.5225

Bozzola, M., & Swanson, T. (2014). Policy implications of climate variability on

agriculture: Water management in the Po river basin, Italy. *Environmental Science & Policy*, *43*, 26–38. https://doi.org/10.1016/j.envsci.2013.12.002

Brenna, A., Bizzi, S., & Surian, N. (2022). A width-based approach to estimating historical changes in coarse sediment fluxes at river reach and network scales. *Earth Surface Processes and Landforms*, *47*(10), 2560–2579. https://doi.org/10.1002/esp.5395

Brenna, A., Bizzi, S., & Surian, N. (2024). How multiple anthropic pressures may lead to unplanned channel patterns: Insights from the evolutionary trajectory of the Po River (Italy). *CATENA*, *234*, 107598. https://doi.org/10.1016/j.catena.2023.107598

Church, M. (2006). BED MATERIAL TRANSPORT AND THE MORPHOLOGY OF ALLUVIAL RIVER CHANNELS. *Annual Review of Earth and Planetary Sciences*, *34*(1), 325–354. https://doi.org/10.1146/annurev.earth.33.092203.122721

Fisher, P. F., & Tate, N. J. (2006). Causes and consequences of error in digital elevation models. *Progress in Physical Geography: Earth and Environment*, *30*(4), 467–489. https://doi.org/10.1191/0309133306pp492ra

Frascaroli, F., Parrinello, G., & Root-Bernstein, M. (2021). Linking contemporary river restoration to economics, technology, politics, and society: Perspectives from a historical case study of the Po River Basin, Italy. *Ambio*, *50*(2), 492–504. https://doi.org/10.1007/s13280-020-01363-3

Khan, S., Fryirs, K., & Bizzi, S. (2021). Modelling sediment (dis)connectivity across a

river network to understand locational-transmission-filter sensitivity for identifying hotspots of potential geomorphic adjustment. *Earth Surface Processes and Landforms*, *46*(14), 2856–2869. https://doi.org/10.1002/esp.5213

Laiolo, P., Gabellani, S., Rebora, N., Rudari, R., Ferraris, L., Ratto, S., Stevenin, H., & Cauduro, M. (2014). Validation of the Flood-PROOFS probabilistic forecasting system. *Hydrological Processes*, *28*(9), 3466–3481. https://doi.org/10.1002/hyp.9888

Lisenby, P. E., & Fryirs, K. A. (2017). 'Out with the Old?' Why coarse spatial datasets are still useful for catchment-scale investigations of sediment (dis)connectivity. *Earth Surface Processes and Landforms*, *42*(10), 1588–1596. https://doi.org/10.1002/esp.4131

Ma, H., Nittrouer, J. A., Naito, K., Fu, X., Zhang, Y., Moodie, A. J., Wang, Y., Wu, B., & Parker, G. (2017). The exceptional sediment load of fine-grained dispersal systems: Example of the Yellow River, China. *Science Advances*, *3*(5), e1603114. https://doi.org/10.1126/sciadv.1603114

Montanari, A. (2012). Hydrology of the Po River: Looking for changing patterns in river discharge. *Hydrology and Earth System Sciences*, *16*(10), 3739–3747. https://doi.org/10.5194/hess-16-3739-2012

Parrinello, G., Bizzi, S., & Surian, N. (2021). The retreat of the delta: A geomorphological history of the Po river basin during the twentieth century. *Water History*, *13*(1), 117–136. https://doi.org/10.1007/s12685-021-00279-3

Pavan, V., Marletto, V., Allodi, A., Antolini, G., & Branchi, M. (n.d.).

COORDINAMENTO TECNICO.

Pelletier, J. D. (2013). 2.3 Fundamental Principles and Techniques of Landscape Evolution Modeling. In *Treatise on Geomorphology* (pp. 29–43). Elsevier. https://doi.org/10.1016/B978-0-12-374739-6.00025-7

Schippa, L., 2021. Studio della morfologia del fondo e degli effetti sul campo di moto e sul trasporto solido nel tratto intermedio del fiume Po. Department of Engineering of University of Ferrara (UNIFE).

Schmitt, R. J. P., Bizzi, S., & Castelletti, A. (2016a). Tracking multiple sediment cascades at the river network scale identifies controls and emerging patterns of sediment connectivity. *Water Resources Research*, *52*(5), 3941–3965. https://doi.org/10.1002/2015WR018097

Schmitt, R. J. P., Bizzi, S., Castelletti, A. F., & Kondolf, G. M. (2018). Stochastic Modeling of Sediment Connectivity for Reconstructing Sand Fluxes and Origins in the Unmonitored Se Kong, Se San, and Sre Pok Tributaries of the Mekong River. *Journal of Geophysical Research: Earth Surface*, *123*(1), 2–25. https://doi.org/10.1002/2016JF004105

Schmitt, R. J. P., Giuliani, M., Bizzi, S., Kondolf, G. M., Daily, G. C., & Castelletti, A. (2021). Strategic basin and delta planning increases the resilience of the Mekong Delta under future uncertainty. *Proceedings of the National Academy of Sciences*, *118*(36), e2026127118. https://doi.org/10.1073/pnas.2026127118

Schoorl, J. M., Sonneveld, M. P. W., & Veldkamp, A. (2000). Three-dimensional landscape process modelling: The effect of DEM resolution. *Earth Surface*

Processes and Landforms, *25*(9), 1025–1034. https://doi.org/10.1002/1096-9837(200008)25:9<1025::AID-ESP116>3.0.CO;2-Z

Schwanghart, W., Groom, G., Kuhn, N. J., & Heckrath, G. (2013). Flow network derivation from a high resolution DEM in a low relief, agrarian landscape. *Earth Surface Processes and Landforms*, *38*(13), 1576–1586. https://doi.org/10.1002/esp.3452

Schwanghart, W., & Scherler, D. (2017). Bumps in river profiles: Uncertainty assessment and smoothing using quantile regression techniques. *Earth Surface Dynamics*, *5*(4), 821–839. https://doi.org/10.5194/esurf-5-821-2017

Surian, N., & Rinaldi, M. (2003). Morphological response to river engineering and management in alluvial channels in Italy. *Geomorphology*, *50*(4), 307–326. https://doi.org/10.1016/S0169-555X(02)00219-2

Tangi, M., Bizzi, S., Fryirs, K., & Castelletti, A. (2022a). A Dynamic, Network Scale Sediment (Dis)Connectivity Model to Reconstruct Historical Sediment Transfer and River Reach Sediment Budgets. *Water Resources Research*, *58*(2), e2021WR030784. https://doi.org/10.1029/2021WR030784

Tarquini, I. Isola, M. Favalli, F. Mazzarini, M. Bisson, M. T. Pareschi, & E. Boschi. (2007). TINITALY/01: A new Triangular Irregular Network of Italy. *Annals of Geophysics*, *50*(3). https://doi.org/10.4401/ag-4424

Temme, A. J. A. M., Schoorl, J. M., Claessens, L., & Veldkamp, A. (2013). 2.13 Quantitative Modeling of Landscape Evolution. In *Treatise on Geomorphology* (pp. 180–200). Elsevier. https://doi.org/10.1016/B978-0-12-374739-6.00039-7

Wohl, E., Brierley, G., Cadol, D., Coulthard, T. J., Covino, T., Fryirs, K. A., Grant, G., Hilton, R. G., Lane, S. N., Magilligan, F. J., Meitzen, K. M., Passalacqua, P., Poeppl, R. E., Rathburn, S. L., & Sklar, L. S. (2019). Connectivity as an emergent property of geomorphic systems. *Earth Surface Processes and Landforms*, *44*(1), 4–26. https://doi.org/10.1002/esp.4434